Study on Dimensional Control of Poly(3-hexylthiophene) and Their Corresponding Applications

胡, 建臣

https://doi.org/10.15017/1398361

出版情報：九州大学, 2013, 博士（工学）, 課程博士
バージョン：

Study on Dimensional Control of Poly(3-hexylthiophene) and Their Corresponding Applications

Hu Jianchen

Supervisor: Wakayama Yutaka

Kyushu University

2013

Content

Chapter 1. Introduction

1.1 Development of polythiophenes (PTs).

1.1.1 Development of unsubstituted PTs

In 1977, Shirakawa and his co-researchers found that iodine (I_2) doped polyacetylene (PA) had conductivity [1], which overturned the conception that polymer could not be utilized as conductive material. Besides, this new discovery extended the application fields of polymer materials and promoted their development. During the passed decades, because of the advantages in easily synthesis, separation and recycling [2, 3], a series of conductive polymers were sequential explored, such as polypyrrole (PPy) [4, 5], polythiophene (PT) [6, 7], polyaniline (PAn) [8, 9], poly(3,4-ethylenedioxythiophene) (PEDOT) [10, 11], and poly(phenylene vinylene) (PPV) [12], etc. Untill now, conductive polymer materials are still attractive, even in many fields they are utilized to replace inorganic materials.

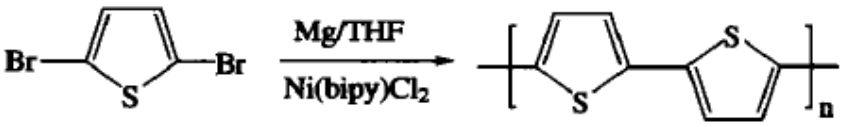

Figure 1-1. Synthesis of polythiophene by using precursor 2,5-Dibromothiophene and metallic catalyst nickel(bipyrine)dichloride ($Ni(bipy)Cl_2$). [13]

In the big family of conductive polymers, semiconductive polymers are currently studied to identify, understand and apply the useful optoelectronic properties inherent in the electron-rich π-systems. Many research groups were inspired to study its properties and to find new, effective semiconductive architectures. Conjugated polymers proved the most durable and robust structures with diverse electronic and physical properties easy to design. Semiconductive polythiophenes (PTs) are such kind of conjugated polymers, possessing the structure like aromatic rings. In 1980, Yamamoto's group [13] firstly synthesized PT by using precursor 2,5-Dibromothiophene and metallic catalyst nickel(bipyrine)dichloride

(Ni(bipy)Cl_2) (Figure 1-1). Then Wochnowski and co-wprkers [14] improved the synthesis method by introducing Uv-vis light as an irradiation source and explained the polymerization mechanism (Figure 1-2).

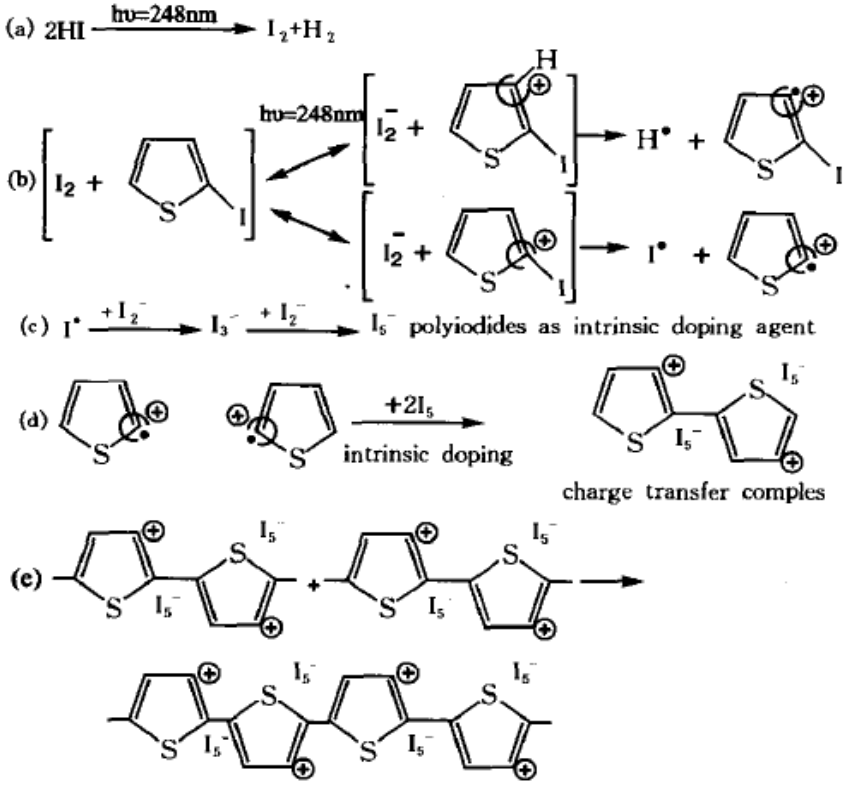

Figure 1-2. Improved process of synthesis of conductive polythiophene by introducing Uv-vis light as an irradiation source. [14]

In PTs, the thiophene rings couple in the 2 and 5 positions, which allows for the conjugation of π orbitals along the polymer chain, leading to the development of semiconductor/insulator band structure for the solid-state materials. That's because the electrophilic reactions favor sites α to the sulfur atom, enchaining predominantly 2,5-couplings to form an extended π-system with quasi one-dimensional delocalization[13]. Higher electrical conductivity in PT can be achieved when the material is oxidized (or doped). The consequence of the oxidation of PT is a prominent change in the electronic

band structure, namely, new midgap states are created and quinoidal type of resonance structure is formed (Figure 1-3). This allows for the production of charge carriers called bipolarons [15]. The oxidation leads to an effective reduction in the band gap and an increase in the electrical conductivity of the material.

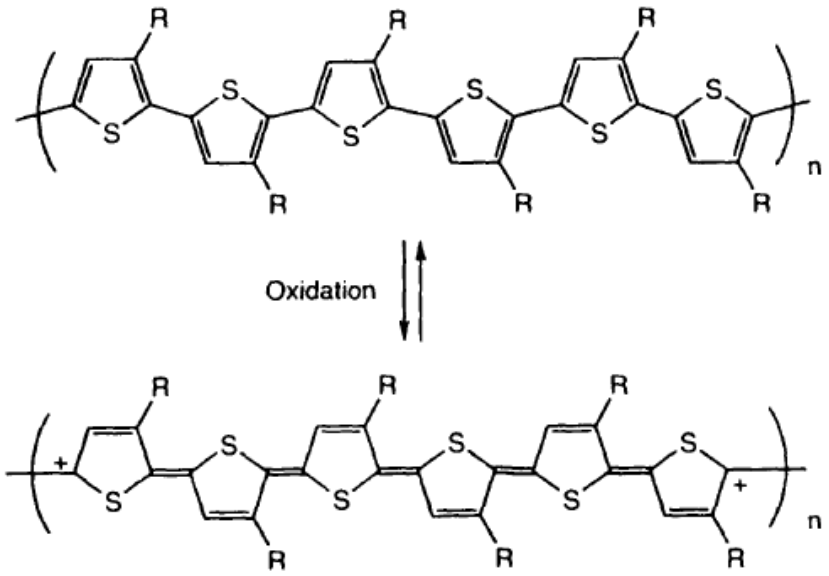

Figure 1-3. Neutral and oxidized forms of polythiophene (R = H or alkyl). [15]

A quinoidal type of resonance structure necessitates that a coplanar orientation of rings be readily accessible, thus a small band gap and high conductivity could be achieved [16]. If high energy constraints prevent the forming coplanar, then a low conductivity will be resulted. In the solide state, electrical conductivity is attributed two aspects: one is dense packing of polymer chains which can allow for overlap to occur in three dimensions (3D) and this 3D conductivity creates low resistivity pathways for carriers (electrons or holes) to travel; the other one is dense chain packing with overlap of the π orbitals which can also lead to high electrical conductivities. In general, the processing of the polymer plays a very important role in controlling the assembly of the 3D structure, determines the polymer morphology, and influences the resulting electrical conductivity [17].

On the other hand, a strong tendency to associate causes some intermolecular overlap but also renders PT insoluble and infusible and therefore difficult to characterize. Yamamoto and co-workers traced this effect to regioisomeric couplings. They developed an exclusively 2,5-coupled PT and found the solubility was negligible. Enchaining 2, 4 defects enabled dissolution but caused backbone twisting, electron localization and widened the optical bandgap [18, 19]. In one word, eliminating couplings β to sulfur resulted in the maximization of effective conjugation length, but formed a material with low processability.

1.1.2 Development of poly(3-alkylthiophene)s (P3ATs)

The insolubility and intractability of PTs, difficult to characterize and study, confined their applications [20]. To extend the practical application of PTs, in the molecular design the molecular propertities should be considered, including the solubility, molecular weight, mechanical strength, stability and, of course, the production cost. Solubility improvement was well realized by adding ring substituents, particularly at 3 position. Because the introduction of ring substituents at 3 position caused the reduction of the interaction between the molecular chains, enabling the increasing of solubility. When the number of carbon atoms of the introduced alkyl or alkoxy substituents is no smaller than 4, the substituted PTs could be dissolved in the solvents like chloroform, tetrahydrofuran (THF), chlorobenzene and N-methyl-2-pyrrolidone (NMP) [21]. The incorporation of 3-alkyl substituents results in a loss of symmetry along the polymer backbone, causing the improvement of processability.

Sugimoto and co-workers reported that $FeCl_3$-mediated polymerization afforded high molecular weight poly(3-alkylthiophene)s (P3ATs) (Mn = 30,000-300,000) [22]. Nevertheless, switching from symmetric thiophene to asymmetric 3-alkylthiophene reintroduces a problem of structural inhomogeneity, which is attributable to regiochemical isomers. This result was obvious observed in the NMR spectrum [23, 24]. The complexity arises from poorly controlled coupling of the asymmetric monomer (Figure 1-4). The chemical environment for a given ring in a homopolymer depends on the orientation of both neighbors, requiring four regioisomeric triads for complete description: head-to-tail

with head-to-tail (HT-HT), tail-to-tail with head-to-head (TT-HH), head-to-tail with head-to-head (HT-HH) and tail-to-tail with head-to-tail (TT-HT). The irregulation of the side chain orientations causes polymer twisting because of the their hindrance. Normally, the twisting confines polymer conjugation and widens the band gap, impacting polymer properties, like conductivity. In contrast, regular (HT-HT) poly(3-alkylthiophene)s are easily to form planar structure with lower band gap and higher conjugation. In addition, these regular P3ATs exihibit fast and large nonlinear optical responses [25, 26], photo- and electroluminescence [27, 28] behavior, and other band gap dependent phoenomena.

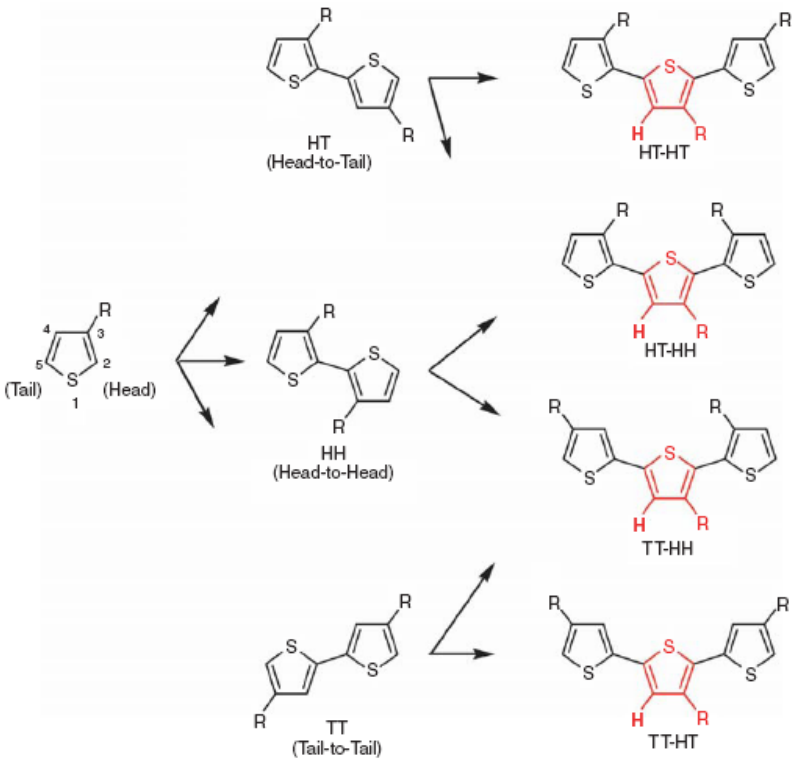

Figure 1-4. Traditional syntheses incorporate multiple regioisomers. [23, 24]

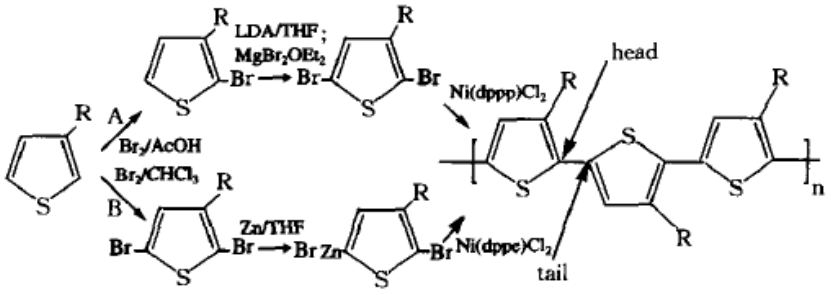

Figure 1-5. Synthesis of regioregular poly(3-alkylthiophene) by McCullough method. [29]

To achieve a high regulation, in 1992, McCullough R K and co-workers [29] firstly reported their synthesis of regioregular P3AT, and the HT regulation was higher than 98% (Figure 1-5). In 1995, they improved the synthesis technology [30] to reduce by-product types and increase productivity of regioregular P3AT with HT structure (Figure 1-6). In 2008, Seung and co-workers improved synthesis process by using active zinc powder under room temperature, reducing the product cost [31].

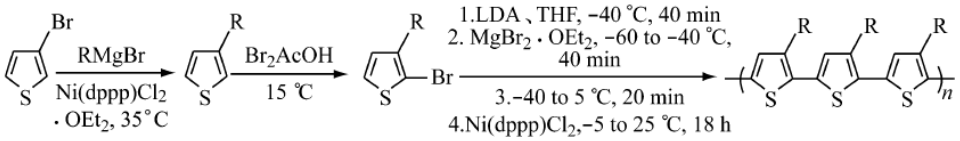

Figure 1-6. Synthesis of regioregular poly(3-alkylthiophene) by improved McCullough method. [30]

In brief, by meaning of introducing ring substituents at 3 position and forming HT regular P3ATs, the solubility is well improved. One the other hand, P3ATs remain the conductivity of unsubstituted PTs [32].

1.2 Electric and photoelectric properties of P3ATs and P3HT

1.2.1 Charge carrier mobility and the influence factors

For organic semiconductors to be valuable in most practical applications, a charge carrier mobility of at least 0.1 $cm^2\ V^{-1}s^{-1}$ is needed (with on/off ratio greater than 10^6) [33]. Bao first report of a relatively high charge carrier mobility for a conjugated polymer was obtained using regioregular poly(3-hexylthiophene) (rr-P3HT), at the level of 0.045 $cm^2\ V^{-1}s^{-1}$ [34]. Later, Sirringhaus improved mobilities in the range 0.05-0.1 $cm^2\ V^{-1}\ s^{-1}$ for rr-P3HT [35]. Regioregularity is critical for good electrical properties [36].

rr-P3HT has been extensively used for studying factors that impact charge carrier mobility, such as processing conditions [37], surface treatment [35] and molecular weight [38]. Generally, the best mobilities are obtained using relatively high molecular weight rr-PHT (*M*n >25 k) under slow evaporating conditions on hydrophobic substrates. These conditions promote self-organization of rr-P3HT with the π–π stacking direction perpendicular to the substrate surface, and also good interconnectivity of crystalline domains [39].

Molecular weight and processing influence the field effect mobility. Zhang *et al.* showed that careful processing of rr-P3HT samples with narrow molecular weight distributions allows assembly into nanofibrils with contour length corresponding to the polymer length [40]. Field effect mobility increased exponentially with nanofibril width. The width of nanofibrils initially increased linearly with *M*w and then leveled off. Yang *et al.* [41] observed nanofibrils for slower cast films of rr-P3HT and the nanofibril width also did not increase with molecular weight above a certain molecular weight threshold. They argued that chain folding limits the nanofibril width and that the resulting entanglements lower crystallinity and mobility [42]. It can be concluded that higher mobility could be obtained if the chain folding could be prevented.

Another important factor that influences mobility in conjugated polymers is charge carrier density: mobility tends to increase with charge carrier density as traps become filled

[43]. Furthermore, when the charge density is sufficiently high, conjugated polymers can reach a very high conductivities like metal-insulator boundary [44].

The studies on effect of side-chain length on field effect mobility suggest that a longer side-chain length is detrimental to field effect mobility. It is suggested that the alkyl side-chains act as a barrier to charge transport between π-conjugated main chains. In 2005, Babel and Jenekhe demonstrated that P3HT was in fact the best, followed by P3BT, P3OT and P3DDT [45].

Both water and oxygen are responsible for the lower on/off ratio, moisture being the dominant factor [46]. High on/off ratios and good stability can be obtained if rr-P3HT is kept under an inert atmosphere [35, 47].

Another related issue with rr-P3HT is its environmental stability. Because of its relatively low ionization potential, rr-P3HT may be susceptible to oxidation in wet air [48]. Furthermore, PTs can undergo photochemical reactions and therefore must be protected from the combination of light and oxygen [49].

In the absence of light, oxygen was not a strong dopant for any of these polymers. Instead, ozone was found to be a strong dopant for PT polymers. Above results explain the variations in stability reported in the literature and suggest that environmental stability studies should be conducted in controlled environments in order to define realistic limits to stability.

The conduction mechanism in polythiophene is the subject of intense investigation [50]. One of the most basic questions still to be answered to understand conductivity and electronic properties in doped PTs remains whether the charge carriers in doped PTs are spinless bipolarons or spin-carrying polaron pairs. Correctly answering this question is crucial for the design and application of PT-based organic semiconductor devices. Initial experimental studies [51] of highly doped PT showed the bipolaron structure to be dominant. Later, this finding was supported by theoretical studies [52].

1.2.2 Exciton Formation by absorption of photon

Inorganic semiconductors have rather high dielectric constant ($\varepsilon > 10$), thus enabling promotion an electron from the valence band to the conduction band by absorbing a photon, resulting in a free electron in the conduction band and a free hole in the valence band. Screened by the surrounding material, these two charge carriers usually do not feel their mutual electrostatic attraction except at very low temperatures under which the kinetic energy of the charge carriers lower than their Coulomb attraction and they form a bound state termed an exciton.

For organic semiconductors, the the dielectric constant is much lower ($\varepsilon \backsimeq$ 3-4), causing the electrostatic attraction between the charge carriers not screened as efficiently. This leads to a much stronger attraction between the charge carriers and ultimately to binding energies of more than 0.5 eV that far exceed the thermal energy at room temperature [53].

At the end of last century, It was argued that whether free charge carriers or bound excitons comprise the primary photoexcitations in conjugated polymers. An agreement was made on that excitons indeed are the primary photoexcitation, mainly because photoexcitation near the bandgap does not directly lead to photoconduction as would have been expected for the generation of free charge carriers [54]. One consequence of this is that optical excitation does not lead to a transition of an electron from the highest occupied molecular orbital (HOMO) to the lowest unoccupied molecular orbital (LUMO), but to a transition to an exciton state that is lower in energy than the LUMO by the binding energy of the exciton.

Three models were found for excitons: Wannier-Mott model was found in inorganic semiconductors and excitons are delocalized over several lattice constants, Frenkel model was found on the basis of excitons are localized on single sites such as small molecules or single conjugated segments of a polymer chain. Charge transfer excitons, comparing to Frenkel excitons, apart from that the two charge carriers are not located on the same site, insteading, on two adjacent sites. These sites can be within the same polymer chain, on two

identical neighboring molecules or even on different adjoining molecules. Depending on the charge carriers spinning orientation, excitons are defined as singlets and triplets, for the former the spins are anti-parallel (total spin 0) and for the latter the spins are parallel (total spin 1). Carbon bonds determine that the ground state of organic molecules is always a singlet state. It is essential to have a change in the symmetry of the wave function for a dipole transition between a ground and an excited state and this change can only be achieved by a change in the angular momentum quantum number ($\Delta l = \pm 1$). A photon involved in such a transition can compensate this change with its spin ($s = 1$), but an additional change in the spin for counteracting is unexpected. This explains why it is spin-forbidden for optical transitions between the singlet ground state and the triplet excited state , also explains optical excitation of organic molecules leads to the formation of singlet excitons. Nevertheless, sometime transitions between singlet and triplet states are available, a precondition of which is that the difference in spin is compensated by the molecule, such as spin-orbit coupling in the presence of heavier atoms like sulfur or by spin-lattice relaxation. This process is termed intersystem crossing and typically occurs on a time scale of 10^{-10} to 10^{-8} s [55].

1.2.3 Formation of Charge-transfer excitons

Preceding section established that in organic semiconductors the formation of a strongly bound singlet exciton by absorption of a photon. Dissociation is essential for obtaining free charge carriers, which can be achieved by blending two organic semiconductors in different energy levels, thus it is favorable for an electron to undergo a charge-transfer process from the bound singlet exciton state to a less tightly bound charge-transfer exciton.

Marcus [56] theoretically intuitively described charge-transfer reactions, and then Jortner [57] extended it to a full many-particle quantum mechanical analysis. The detailed introduction to charge-transfer theory can be found in reference [58].

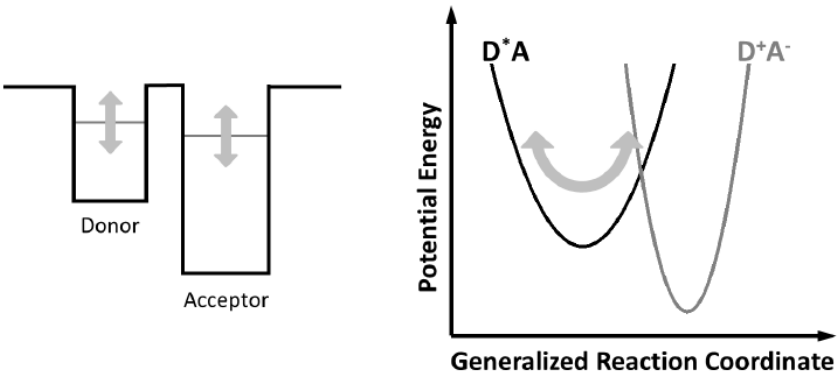

Figure 1-7. Quantum well and potential energy surfaces relevant for charge transfer. Arrows indicate fluctuations about the generalized reaction coordinate leading to changes in the energy levels of the quantum wells which corresponds to oscillations along the potential energy surface [58].

A simplified quasi one particle model was established to describe the movement of an electron in the potential energy landscape created by the atomic nuclei of the donor and the acceptor sites involved in the transfer of an electron from an excited donor site *D** to an acceptor site *A* in the form $D^*A \rightarrow D^+A^-$. This potential energy landscape essentially creates donor and acceptor quantum wells with width and depth depending on the momentary configuration of the atomic nuclei. Such quantum wells along with the corresponding electronic energy levels are illustrated on the left side of Figure 1-7. Assuming no energy exchange between the electron and its environment, the electronic energy levels of the donor and the acceptor have to be equal in order to satisfy the conservation of energy during the transfer. Consequently, all nuclei involved in the transfer process have to reorganize by statistical fluctuations about their equilibrium positions, by meaning of which the energy levels in the donor and the acceptor quantum well match. This can also be illustrated with the help of so called potential energy surfaces. On the right side of Figure 1-7 these potential energy surfaces before (labeled *D*A*) and after charge transfer (labeled

D^+A^-) are represented by parabolas plotted against a generalized reaction coordinate accounting for all degrees of freedom of the nuclear configurations. As indicated by arrows in Figure 1-7, vibrations, rotations and similar fluctuations of the nuclei cause the system to oscillate along the potential energy surface D^*A. When the system reaches the point where the energy of the states before and after charge separation are identical (link of the parabolas), charge transfer can occur.

In classical Marcus theory the molecular fluctuations along a potential energy surface are described by harmonic oscillations about an equilibrium position (minimum of a parabola). Figure 1-8 shows the definition of the parameters used for describing the problem. Both potential surfaces are assumed to be parabolas with identical curvature c. The equilibrium configurations of the initial ($D^*A(q) = cq^2 + G_{D^*A}$) and of the charge transferred ($D^+A^-(q) = c(q-\Delta)^2 + G_{D^+A^-}$) states are denoted with $q = 0$ and $q = \Delta$ and they are energetically displaced by the value of $G^* = G_{D^*A} - G_{D^+A^-}$. G_B^* is the energy barrier the system needs to overcome before charge transfer can occur and G_X is the intersection of the parabolas. The reorganization energy $\lambda = D^*A(\Delta) - D^*A(0) = c\Delta^2$ is defined as the amount of energy that would be needed to change the molecular configuration of the initial state to that of the equilibrium position Δ of the charge transferred state. It can be divided into a so called inner sphere describing the contribution of the molecule(s) directly involved in the transfer process and outer sphere contribution referring to all molecules in the closer vicinity of the directly involved molecule(s). In other words, through the formalism of reorganization Marcus' theory explicitly takes the polaronic nature of charge carriers into account by considering the energy it takes for a charge carrier to move its associated lattice distortion along during the transfer process. All energies mentioned here are Gibbs free energies to account for entropic effects.

From geometrical considerations, the energy barrier is given by $G_B = \frac{(\lambda+G^*)^2}{4\lambda}$. While the reorganization of the system directly forms a barrier for charge transfer, the influence of the energetic displacement G^* of the equilibrium configurations is a bit more complicated. In the regime $0>G^*\geq-\lambda$ it acts as a driving force for charge transfer by decreasing the energy

barrier. However, if the absolute value of G^* exceeds λ, $G^* < -\lambda$, it has the opposite effect and increases the barrier. In thermodynamic equilibrium the charge-transfer rate of the system can be determined by Boltzmann statistics as

$$k_{CT} = A\exp[-\frac{G_B}{k_B T}] = A\exp[-\frac{(G^*-\lambda)^2}{4\lambda k_B T}] \qquad (1\text{-}1)$$

with Boltzmann's constant k, at Temperature T, and with the coupling constant A that depends on the specific type of transfer reaction (e.g. intra- or intermolecular transfer).

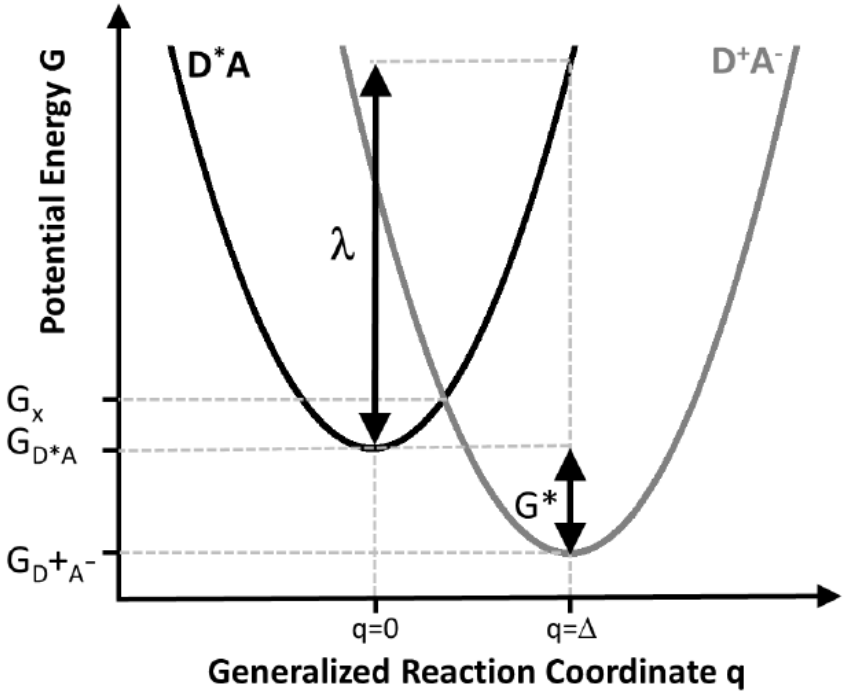

Figure 1-8. Potential energy surfaces of the initial (D^*A) and the charge transferred (D^+A^-) state approximated by parabolas. [58]

In some cases not every site in a material is suitable for charge transfer so that an additional transport step precedes the transfer process. Comparing to the actual transfer time, if this transport step is slow the overall rate of the transfer process is reduced. For a transport mechanism of three dimensional isotropic diffusion an estimation of the reduced transfer rate can be obtained. Assuming an excitation has to travel a distance x on average between the site where it was created and a site suitable for charge transfer, the average rate k_D for the excitation to reach a transfer site is given by

$$k_D = \frac{D}{x^2} \tag{1-2}$$

with diffusion constant D. The total charge-transfer rate k_{CT} in the limit of very fast transfer and very slow diffusion can be approximated by the diffusion rate $k_{CT} \approx k_D$. If the phases segregate of blending organic semiconductors form large, pure domains so that the diffusion time of excitons to the interface between the phases is larger than the duration of the charge-transfer process itself, diffusion limited charge transfer can be found. For a diffusion constant of $D = 10^{-3}$ cm²/s and assuming that the charge-transfer time is lower than 100 fs, an average diffusion distance of as little as 0.1 nm will lead to a diffusion limited charge-transfer rate [59]. In blends for efficient organic solar cells domain sizes usually exceed 1 nm, so it seems likely that diffusion indeed limits the charge-transfer rates in such systems. Cowan *et al.* recently argued that for organic solar cells, excitons in donor-polymers are initially highly delocalized and relax into more localized excitons on a timescale comparable to charge transfer. Such an initial delocalization has effect on increasing the critical domain size at which diffusion effects start to become important.

1.2.4 Charge Separation: Dissociation of Charge-transfer excitons

The morphology have a huge influence on the separation of charge-transfer excitons in various ways and consequently on a broad range of length scales. These scales range from the orientation of molecules at the interface to the formation of interpenetrating phase

segregated networks of blended materials. A variety of methods for controlling the morphology have been developed experimentally. Among these are variations of the sample preparation conditions, like using different solvents [60] or annealing conditions [61], introducing smaller modifications in the molecular structure like a replacement of side-chains [62]. All of these approaches have in common that they involve rather subtle changes within a series of samples under study in order to keep secondary effects that could influence charge separation

Two processes determine the optimal size for nanoscale phase segregation in terms of charge separation. One is an upper limit given by the exciton diffusion length. If the phase domains are larger than this diffusion length, not all excitons will reach the interface to undergo charge transfer but will recombine insteadly. On the other hand the charge carriers have to be able to move far enough from the interface to be considered spatially separated.

Veldman and Quist found that the larger phase segregation is beneficial for the dissociation of charge-transfer excitons. Annealing in P3HT:PCBM was found to have a similar effect [61] and the simultaneous recovery of the photoluminescence [62], indicating an incomplete exciton quenching. These results further supported the conclusion that larger pure phase domains lead to a more facile dissociation of charge-transfer excitons.

Holcombe *et al.* [63] found that a larger distance between the donor and acceptor molecules resulted in a reduced charge-transfer exciton binding energy and a higher dissociation probability, showing that the precise interfacial structure strongly impacts the formation of spatially separated charges.

Liu *et al.* performed molecular dynamics simulations explicitly accounting for structural variability at the interface of P3HT:PCBM [64]. They concluded that either charge separated states or charge bridging states that can be assigned to charge-transfer excitons can be formed after the dissociation of a singlet exciton at the interface depending on the exact interface geometry.

Further theoretical calculations and experiments suggest that certain molecular arrangements can cause the formation of dipoles at the interface which can reduce the Coulombic attraction between an electron and a hole in a charge-transfer exciton, thus the dissociation probability increase [65].

1.2.5 Charge Transport

Charge transport repeats itself in the physical mechanisms as an omnipresent motif, which govern the device performance of organic solar cells. That is the reason why a detailed understanding of the underlying principles of charge transport is very important when trying to correlate molecular structures, charge transport properties and device performance.

Unlike inorganic semiconductors, organic semiconductors have no translational symmetry, but instead they have an ensemble of localized sites with slightly varying energetic levels and distances between them. Bässler [60] observed the sites that are very low in energy can act as traps for charge carriers, because they accept charge carriers very quickly but release them only slowly. Spatially isolated sites however cannot trap charges as efficiently because of the symmetry of the trapping and detrapping rates [61].

It was also found that [62] at high temperatures the charge carriers created in a sample can equilibrate within the density of states much faster than their average transit time through the sample. Consequently, the average charge carrier mobility obtained from an experiment is dependent of the equilibrium charge carrier mobility and is independent of the sample thickness.

At the temperature below critical temperature (*Tc*) the time needed for equilibration is longer than the transit time of charge carriers through the sample. This means that the charge carrier mobility determined from an experiment would no longer be the equilibrium charge carrier mobility, and the actual value would strongly depend on the sample thickness.

These two regimes of charge transport are termed non-dispersive and dispersive charge transport, respectively.

1.2.6 Charge carriers recombination

The most basic requirement for recombination of independently moving opposite charge carriers (i.e. electrons and holes) is that they approach each other close enough to enter their mutual capture radius. This random process is basically dominated by the probability of two charge carriers meeting. This kind of recombination was first described by Langevin [53] for the recombination of ions in gases.

An important requirement for Langevin recombination to be applicable is that the mean free path of a charge carrier (i.e. the typical length scale of the motion of a charge carrier) is much shorter than the capture radius of two opposite charges. The typical length scale of charge motion in organic semiconductors can be considered to be limited either by the dimension of the conjugated system of the site or by the hopping distance between neighboring sites. In any case it is well below the Coulomb capture radius of more than 10 nm, so that this prerequisite can be considered fulfilled in disordered organic semiconductors.

Essentially, the recombination rate increases if there are more charge carriers and if the charge carriers move faster. In blends of organic semiconductors, as used for solar cell devices, electrons and holes are each confined to one of the material phases, thus recombination can only occur at an interface. This effectively decreases the recombination rate.

As has been pointed out by Juska *et al*. [63], the reaction order of the recombination can also be limited by the dimensionality of the charge carrier motion.

In brief, recombination strongly depend on the exact morphology of a sample that can be influenced not only by material properties but also by sample preparation conditions.

1.3 Current issues of P3HT applications

After the development of more than 20 years, synthesis of P3ATs is already industrialized. The applications are also extened to many fields. Among them, poly-3-hexylthiophene (P3HT) is one of the most extensively studied conjugated polymer because

of its relatively high carrier mobility coupled with solution processability [34, 35].

P3HT applications run from light-emitting diodes [70] to thin-film transistors [71]. Moreover, P3HT coupled with inorganic materials (e.g. TiO_2 [72], ZnO [73], carbon nanotubes [74], phenyl-C61-butyric acid methyl ester [75]) is an excellent component for use in low-cost photovoltaics. Polythiophene-based solar cells have reached power conversion efficiencies of about 7.4% [76].

The applications of P3HT are mainly based on its electrical and photoelectric properties, especially in the application of solar cell and improvement of its conductivity. Nevertheless, there are still some issues to be settled:

(1) For fabrication of P3HT-base organic solar cell, the spin coating method has been established as the most reliable and reproducible process using the solution process. However, material waste is unavoidable in spin coating process. Moreover, this method is only suitable for a limited substrate size. For the future application of polymer solar cells (PSCs), somethings should be considered about, such like the production cost should be minimized, the producing process should be continuous and a high throughput should be achieved. Besides, the technique should be able transfer to the flexible substrates with large area, which is the main advantage of PSCs. During the passed decades, new deposition techniques have been demonstrated for PSC fabrication including ink-jet printing, spray coating, and screen printing. Each method was proposed to avoid the disadvantages of spin coating technique, but unfortunately, all these techniques require costly equipment. In contrast, the dip coating technique has been developed as a cost effective method but it cannot be applied to soft substrates because organic solvent may dissolve the plastic substrate during solution processes. Therefore, new technique should be found to fabricate large-scale PSCs at low cost with inexpensive equipment and little material waste. Moreover, the improved technique should be easily applicable to soft substrates such as polyethylene terephthalate.

(2) Development of effective fabrication techniques to produce polymer solar cell is one aspect for the further application. On the other hand, cell performance is the most important

parameter to evaluate the application prospect. The high performance should be harvested from the cells designed and prepared on the basis of well understanding of the material properties. Bulk heterojunction (BHJ) solar cells, the most reliable representative, are superior to single- and double-layer cells. The BHJ structure can be formed simply by mixing a donor and acceptor solution. This straightforward technique is advantageous in terms of increasing the donor/acceptor (D/A) interface, which provides the exciton dissociation sites. Meanwhile, a weak point as regards BHJs is that the pathways of the generated carriers are not ensured because of the random phase separation of the respective materials, namely, isolated domains may exist in each other. To ensure exciton dissociation and carrier collection, continuous percolation pathways are required.

An ideal structure would be an interdigitated interface, where the donor and acceptor phases are separate. The diameter and interspatial distance of the pillars should preferably be comparable to the diffusion length of the excitons, which is of the order of 10 nm. Then, the excitons can diffuse to the D/A interface during their lifetime. Furthermore, the interdigitated structure must be aligned perpendicularly to connect with the electrodes so as to provide direct pathways for efficient charge transportation. Meanwhile, the film thicknesses should be around 100 to 200 nm to absorb the incident light and to confine the series resistance. For these reasons, the dimensions of the interdigitated structures should be carefully designed to enhance photovoltaic effects. Interdigitated structures have been obtained using different techniques including self-organization and nanoimprinting. However, there is still room for further optimization of the dimensions.

(3) Poly(3-hexylthiophene) (P3HT) has high field-effect mobility of 0.2 $cm^2V^{-1}s^{-1}$, which is the highest reported for a polymer. Such a high mobility is caused by the formation of a lamellar structure by the self assembly of alkyl side chains. Except head-tail (H-T) regioregularity, the conductivity of P3HT depends on processing condition; e.g., the spin-coated samples have 2 orders higher conductivity than that of the solvent-cast film. However, for organic semiconducting devices molecular doping is preferable, since field-induced drift of the relative large-size charged molecular dopants can be suppressed. By

using iodine (I_2) as dopant the conduction in P3HT films could be enhanced, but different doping level should be performed by different techniques. Furthermore, in regionrandom P3HT (RRa-P3HT) the doping level achieved was found be higher than that in regioregular P3HT (RR-P3HT), indicating that I_2 was absorbed more deeply into RRa-P3HT than RR-P3HT. But RR-P3HT is much more popular in most applications because its better electrical properties. Recently, P3HT based OFETs doped with the strong acceptor 2,3,5,6-tetrafluoro-7,7,8,8-tetracyanoquinodimethane (F4-TCNQ) have been reported, in which P3HT works as a hole transport material. Meanwhile, F4-TCNQ can function as acceptors that increase the hole density owing to the high electron affinity of cyano groups and fluorine atoms. A advantage for F4-TCNQ is that it can be dissolved together with P3HT. In these applications, a challenging task is to achieve uniform doping and thus improve the conductivity of P3HT. Besides, because of the dismatch of P3HT and dopant, the doping level is always limited.

1.4 Strategies proposed in this thesis and their motivations

Material properties decide the possibilities of the material applications. In the applications, the preference of the material properties should be maximized. As an example, the electrical and photoelectric properties of organic semiconductors make it possible to apply these materials in many fields like discussed in Section 1.2 and 1.3. P3HT, a typical representative, was widely studied in many fields, especially in organic field effect transistor and organic solar cell. In organic devices, morphology strongly influences device properties, since the morphology can impact on the material electrical or photoelectric properties, such as carrier mobility, exicton generation and dissociation, carrier transportation and recombination. Therefore, in the relevant applications, reasonable designs on device structure, particularly nanostructure, are essential for improving device performances. On the basis of these reasons, in this thesis, we focus on the dimensional control, sub-1D, 1D and 2D, of P3HT in nanoscale and verify their applications in the relevant fields.

(1) Fabrication of sub-1D P3HT nanopillars and the application in organic solar cell

We employed an anodic aluminum oxide (AAO) template to prepare a poly(3-hexylthiophene) (P3HT)/fullerene (C_{60}) interdigitated structure to enlarge the D/A interface. P3HT absorbs the light from 400 to 700 nm to generate excitons. Meanwhile, C_{60} absorbs the light in the UV range of 300 to 400 nm and acts as an electron acceptor to transport such electrons to the electrode. This strategy has the following merits: Firstly, the sub-1D pillar size can be well controlled as regards diameter, interval, and height, making it close to the exciton diffusion length. Secondly, because the pillars and the P3HT film are integrated, a carrier pathway can be formed, which is directly connected to the electrodes. Finally, self-standing pillars can be fabricated uniformly over a large area. Besides, because of the phase separation, no isolated domains exist. With this technology, costly imprinting equipment and cumbersome processes like dry etching are avoidable.

(2) Fabrication of 1D P3HT nanowires doped with dopant and the improvement in conductivity

We employed AAO as templates to fabricate 1D P3HT nanowires doped with F4-TCNQ. A great advantage of the AAO template is that a large number of nanowires with a uniform diameter and length can be readily produced. In this strategy, the capillary force in the nanopores of the AAO template compels the chemical dopants to mix into the main matrix at a high doping level, resulting in enhanced conductivity in the molecular nanowires. Such high conductivity is not achievable with the conventional two-dimensional (2D) thin film geometry due to dopant segregation.

Methodologically, to measure the resistivity in individual nanowires precisely, we employed a four-probe scanning tunneling microscope (STM), which was integrated with a scanning electron microscope (SEM). The four-probe STM technique has significant benefits in providing stable contacts, suppressing the contact resistance effect, accessing individual measurement nano-objects, and especially in allowing multiple measurements on the same nanowires. Results show that the resistivities of P3HT/F4-TCNQ nanowires were

tuned in the range of 0.1-10 Ωcm by changing the F4-TCNQ concentration from 10 to 0.1 wt., which were 2-4 orders of magnitude smaller than those of the corresponding P3HT/F4-TNCQ thin film composites. In contrast, the resistivities of F4-TCNQ doped P3HT films were around 4-5 × 10^3 Ωcm, almost independent of the F4-TCNQ concentration.

(3) Fabrication of 2D ITO/PEDOT:PSS/P3HT:PCBM mutilayered structure with a one-step technique and its application in solar cell

We described a one-step fabrication technique for large-scale indium tin oxide/poly(3,4-ethylenedioxythiophene):poly(styrenesulfonate)/ poly(3-hexylthiophene-2,5-diyl):[6,6]-phenyl-C61-butyric acid methyl ester (ITO/ PEDOT:PSS/P3HT:PCBM) multi-layered structures that uses a solution process. The structure was formed by droping P3HT:PCBM solution on the surface of PEDOT:PSS solution in which ITO/glass substrate was immersed. After solvent evaporation, the substrate was picked up and thus the formed P3HT:PCBM films could be transferred to the PEDOT:PSS covered substrate. We show that this process is achievable under very simple conditions. Several motivations could be attained by this method: simple method, inexpensive equipment, no material waste, thickness controllable and large area. Preliminary device properties show that the fabricated structure can be used for organic solar cells.

References

[1] Shirakawa, H; Louis, E. J.; MacDiarmid , A. G.; Chiang C. K.; Heeger, A. J. Synthesis of Electrically Conducting Organic Polymers: Halogen Derivatives of Polyacetylene, $(CH)_x$. *J. Chem. Soc., Chem. Commun.* **1977**, *16*, 578-580.

[2] Hiraishi, K.; Masuhara, A.; Nakanishi, H.; Oikawa, H.; Shinohara, Y. Evaluation of Thermoelectric Properties of Polythiophene Films Synthesized by Electrolytic Polymerization. *Jpn. J. Appl. Phys.* **2009**, *48*, 0715011-0715014.

[3] Shinohara, Y.; Ohara, K.; Nakanishi, H.; Imai, Y.; Isoda, Y. Thermoelectric Properties of Poly(3- alkylthiophenes). *Mater. Sci. Forum* **2005**, *492- 493*, 141-144.

[4] Diaz, A. F.; Castillo, J. I.; Logan, J. A.; Lee, W. Y. Electrochemistry of Conducting Polypyrrole Films. *J. Electroanal. Chem.* **1981**, *129*, 115-132.

[5] Li, X. G.; Li, A.; Huang, M. R.; Liao, Y.; Lu, Y. G. Efficient and Scalable Synthesis of Pure Polypyrrole Nanoparticles Applicable for Advanced Nanocomposites and Carbon Nanoparticles. *J. Phys. Chem. C* **2010**, *114*, 19244-19255.

[6] Li, X. G.; Li, J.; Huang, M. R. Facile Optimal Synthesis of Inherently Electroconductive Polythiophene Nanoparticles. *Chem.-Eur. J.* **2009**, *15*, 6446- 6455.

[7] Waltman, R.; Bargon, J.; Diaz, A. Electrochemical Studies of Some Conducting Polythiophene Films. *J. Phys. Chem.* **1983**, *87*, 1459-1463.

[8] Macdiarmid, A. G.; Chiang, J. C.; Richter, A. F. Polyaniline: A new Concept in Conducting Polymers. *Synth. Met.* **1987**, *18*, 285-290.

[9] Li, X. G.; Huang, M. R.; Duan, W.; Yang, Y. L. Novel Multifunctional Polymers from Aromatic Diamines by Oxidative Polymerizations. *Chem. Rev.* **2002**, *102*, 2925-3030.

[10] Greczynski, G.; Kugler, T.; Salaneck, W. Characterization of the PEDOT-PSS System by Means of X-ray and Ultraviolet Photoelectron Spectroscopy. *Thin Solid Films* **1999**, *354*, 129-135.

[11] Choi, J.; Cho, K.; Yim, J. Micro-patterning of Vapor-phase Polymerized Poly (3, 4-ethylenedioxy thiophene) (PEDOT) Using Ink-jet Printing/Soft Lithography. *Eur. Polym. J.* **2010**, *46*, 389-396.

[12] Cernini, R.; Li, X. C.; Spencer, G. W. C.; Holmes, A. B.; Moratti, S. C.; Friend, R. H. Electrochemical and Optical Studies of PPV Derivatives and Poly(aromaticox adiazoles). *Synth. Met.* **1997**, *84*, 359-360.

[13] Yamamoto, T.; Sanechika, K.; Yamamoto, A. Preparation of Thermostable and Electric-conducting Poly(2,5-thienylene). *J. Poly. Sci. Polym. Lett. Ed.* **1980**, *18*, 9-12.

[14] Wochnowski, C.; Metev, S. UV-laser-assisted Synthesis of Iodine-doped Electrical Conductive Polythiophene. *Appl. Surf. Sci.* **2002**, *186*, 34-39.

[15] Bredas, J. L.; Street, G. B. Polarons, Bipolarons, and Solitons in Conducting Polymers. *Acc. Chem. Res.* **1985**, *18*, 309-315.

[16] Baughman, R. H.; Bredas, J. L.; chance, R. R.; Elsenbaumer, R. L.; Shacklette, L. W. Structural Basis for Semiconducting and Metallic Polymer Dopant Systems. *Chem. Rev.* **1982**, *82*, 209-222.

[17] Moulton, J.; Smith, P. Electrical and Mechanical Properties of Oriented Poly(3-alkylthiophenes): 2. Effect of Side-chain Length. *Polymer* **1992**, *33*, 2340-2347.

[18] Yamamoto, T.; Sanechika, K.; Yamamoto, A. Preparation of Poly(2,4-thienylene) and Comparison of Its Optical and Electrical Properties with Those of Poly(2,5-thienylene). *Chem. Lett.* **1981**, *8*, 1079-1082.

[19] Sanechika, K.; Yamamoto T.; Yamamoto, A. Preparation of Copolymers Composed of 2,5-thienylene and 2,4-thienylene Units. Effect of Copolymer Composition on Electronic

Spectrum, Electric Conductivity and Chemical Properties. *J. Polym. Sci., Polym. Lett. Ed.* **1982**, *20*, 365-371.

[20] Jen, K. Y.; Miller, G. G.; Elsenbaudemr, R. L. Highly Conducting, Soluble, and Environmentally-stable Poly(3-alkylthiophenes). *J. Chem. Soc., Chem. Commun.* **l986**, *17*, 1346-1347.

[21] Wang, Y.; Lucht, B. L.; Euler, W. B. Investigation of the Oxidative Coupling Polymerization of 3-alkylthiophenes with Iron(III) Chloride. *Polymer preprints* **2002**, *43*, 1160.

[22] Sugimoto, R.; Takeda, S.; Gu, H. B.; Yoshino, K. Preparation of Soluble Polythiophene Derivatives Utilizing Transition Metal halides as Catalysts and Their Property. *Chem. Express* **1986**, *1*, 635-638.

[23] Aime, J. P.; Bargain, F.; Schott, M.; Eckhardt, H.; Miller, G. G.; Elsenbaumer, R. L. Structural Study of Doped and Undoped Polythiophene in Solution by Small-angle Neutron Scattering. *Phys. Rev. Lett.* **1989**, *62*, 55–58.

[24] Sato, M.; Morii, H. Nuclear Magnetic Resonance Studies on Electrochemically Prepared Poly(3-dodecylthiophene). *Macromolecules* **1991**, *24*, 1196–1200.

[25] Daoud, W. A.; Xin, J. H.; Regioregular Poly(3-alkylthiophenes): Synthesis, Characterization, and Application in Conductive Fabrics. *J. Appl. Polym. Sci.* **2004**, *93*, 2131-2135.

[26] Williams, D. J. Organic Polymeric and Non-Polymeric Materials with Large Optical Nonlinearities. *Angew. Chem., Int. Ed.* **1984**, *23*, 690-703.

[27] Burroughes, J. H.; Bradley, D. D. C.; Brown, A. R.; Marks, R. N.; Mackay, K.; Friend, R. H.; Burns, P. L.; Holmes, A. B. Light-emitting diodes based on conjugated polymers. *Nature*, **1990**, *347*, 539-541.

[28] Xu, B.; Holdcroft, S. Molecular Control of Luminescence from Poly(3-hexylthiophenes). *Macromolecules* **1993**, *26*, 4457-4460.

[29] McCullough, R. D.; Lowe, R. D. Enhanced Electrical Conductivity in Regioselectively Synthesized Poly(3-alkylthiophenes). *J. Chem. Soc., Chem. Commun.* **1992**, *1*, 70-72.

[30] McCullough, R. D.; Williams, S. P.; Nagles, S. T.; Jayaraman, M.; Ewbank, P. C.; Miller, L. The First Synthesis and New Properties of Regioregular, Head-to-tail Coupled Polythiophenes. *Synth. Met.* **1995**, *69*, 279-282.

[31] Kim, S. H.; Kim, J. G. A Practical Approach for the Preparation of Regioregular Poly(3-hexylthiophene). *B. Kor. Chem. Soc.* **2010**, *31*, 193-195.

[32] McCullough R. D.; Lowe, R. D.; Jayaraman, M; Anderson, D. L.Design, Synthesis, and Control of Conducting Polymer Architectures: Structurally Homogeneous Poly(3-alkylthiophenes). *J. Org. Chem.* **1993**, *58*, 904-912.

[33] Katz, H. E.; Bao, Z. The Physical Chemistry of Organic Field-effect Transistors. *J. Phys. Chem. B* **2000**, *104*, 671-678.

[34] Bao, Z.; Dodabalapur, A.; Lovinger, A. J. Soluble and Processable Regioregular Poly(3-hexylthiophene) for Thin Film Field-effect Transistor Applications with High Mobility. *Appl. Phys. Lett.* **1996**, *69*, 4108-4110.

[35] Sirringhaus, H.; Tessler, N.; Friend, R. H. Integrated Optoelectronic Devices Based onConjugated Polymers. *Science* **1998**, *280*, 1741-1744.

[36] Assadi, A.; Svensson, C.; Willander, M.; Inganas, O. Field-effect Mobility of Poly(3-hexylthiophene). *Appl. Phys. Lett.* **1988**, *53*, 195-197.

[37] Chang, J. F.; Sun, B.; Breiby, D. W.; Nielsen, M. M.; Soelling, T. I.; Giles, M.; McCulloch, I.; Sirringhaus, H. Enhanced Mobility of Poly(3-hexylthiophene) Transistors by Spin-coating from High-boiling-point Solvents. *Chem. Mater.* **2004**, *16*, 4772-4776.

[38] Zen, A.; Saphiannikova, M.; Neher, D.; Grenzer, J.; Grigorian, S.; Pietsch, U.; Asawapirom, U.; Janietz, S.; Scherf, U.; Lieberwirth, I.; Wegner, G. Effect of Molecular Weight on the Structure and Crystallinity of Poly(3-hexylthiophene). *Macromolecules* **2006**, *39*, 2162-2171.

[39] Chang, J. F.; Clark, J.; Zhao, N.; Sirringhaus, H.; Breiby, D. W.; Andreasen, J. W.;

Nielsen, M. M.; Giles, M.; Heeney, M.; McCulloch, I. Molecular-weight Dependence of Inter-chain Polaron Delocalization and Exciton Bandwidth in High-mobility Conjugated Polymers. *Phys. Rev. B.: Condens. Matter Mater. Phys.* **2006**, *74*, 115318/1-115318/12.

[40] Zhang, R.; Li, B.; Iovu, M. C.; Jeffries-El, M.; Sauve, G.; Cooper, J.; Jia, S.; Tristram-Nagle, S.; Smilgies, D. M.; Lambeth, D. N.; McCullough, R. D.; Kowalewski, T. Nanostructure Dependence of Field-effect Mobility in Regioregular Poly(3-hexylthiophene) Thin Film Field Effect Transistors. *J. Am. Chem. Soc.* **2006**, *128*, 3480-3481.

[41] Yang, H.; Shin, T. J.; Bao, Z.; Ryu, C. Y. Structural Transitions of Nanocrystalline Domains in Regioregular Poly(3-hexyl thiophene) Thin Films. *J. Polym. Sci. Part B: Polym. Phys.* **2007**, *45*, 1303-1312.

[42] Mena-Osteritz, E.; Meyer, A.; Langeveld-Voss, B. M. W.; Janssen, R. A. J.; Meijer, E. W.; Bauerle, P. Two-dimensional Crystals of Poly(3-alkylthiophene)s: Direct Visualization of Polymer Folds in Submolecular Resolution.*Angew. Chem. Int. Ed.* **2000**, *39*, 2680-2684.

[43] Pasveer, W. F.; Cottaar, J.; Tanase, C.; Coehoorn, R.; Bobbert, P. A.; Blom, P. W. M.; de Leeuw, D. M.; Michels, M. A. J. Unified Description of Charge-carrier Mobilities in Disordered Semiconducting Polymers. *Phys. Rev. Lett.* **2005**, *94*, 206601/1-206601/4.

[44] Heeger, A. J. Semiconducting and Metallic Polymers: the Fourth Generation of Polymeric Materials. *Synth. Met.* **2002**, *125*, 23-42.

[45] Babel, A.; Jenekhe, S. A. Alkyl Chain Length Dependence of the Field-effect Carrier Mobility in Regioregular Poly(3-alkylthiophene)s. *Synth. Met.* **2005**, *148*, 169-173.

[46] Hoshino, S.; Yoshida, M.; Uemura, S.; Kodzasa, T.; Takada, N.; Kamata, T.; Yase, K. Influence of Moisture on Device Characteristics of Polythiophene-based Field-effect Transistors. *J. Appl. Phys.* **2004**, *95*, 5088-5093.

[47] Hamadani, B. H.; Natelson, D. Gated Nonlinear Transport in Organic Polymer Field Effect Transistors. *J. Appl. Phys.* **2004**, *95*, 1227-1232.

[48] de Leeuw, D. M.; Simenon, M. M. J.; Brown, A. R.; Einerhand, R. E. F. Stability of n-type Doped Conducting Polymers and Consequences for Polymeric Microelectronic Devices. *Synth. Met.* **1997**, 87, 53-59.

[49] Abdou, M. S. A.; Holdcroft, S. Mechanisms of Photodegradation of Poly(3-

alkylthiophene)s in Solution. *Macromolecules* **1993**, *26*, 2954-2962.

[50] Barta, P.; Cacialli, F.; Friend, R. H.; Zagorska, M. Efficient Photo and Electroluminescence of Regioregular Poly(alkylthiophene)s. *J. Appl. Phys.* **1998**, *84*, 6279-6284.

[51] Dodabalapur, A.; Bao, Z.; Makhija, A.; Laquindanum, J. G.; Raju, V. R.; Feng, Y.; Katz, H. E.; Rogers, J. Organic Smart Pixels. *Appl. Phys. Lett.* **1998**, *73*, 142-144.

[52] Chen, T. A.; Wu, X.; Rieke, R. D. Regiocontrolled Synthesis of Poly(3-alkylthiophenes) Mediated by Rieke Zinc: Their Characterization and Solid-state Properties. *J. Am. Chem. Soc.* **1995**, *117*, 233-244.

[53] Pope, M.; Swenberg, C. E. Electronic Processes in Organic Crystals and Polymers. Oxfor University Press: New York, **1999**.

[54] Lochner, K.; Bässler, H.; Tieke, B.; Wegner, G. Photoconduction in Polydiacetylene Multilayer Structures and Single Crystals. Evidence for Band-to-Band Excitation. *Phys. Status. Solidi. B* **1978**, *88*, 653-661.

[55] Valeur, B. Molecular Fluoresence: Principles and applications. *Wiley-VCH: Weinheim* **2002**.

[56] Marcus, R. A. On the Theory of Oxidation-Reduction Reactions Involving Electron Transfer. I. *J. Chem. Phys.* **1956**, *24*, 966-978.

[57] Jortner, J. Temperature Dependent Activation Energy for Electron Transfer between Biological Molecules. *J. Chem. Phys.* **1976**, *64*, 4860-4867.

[58] May, V.; Kühn, O. Charge and Energy Transfer Dynamics in Molecular Systems; 1 ed.. *Wiley-VCH Verlag GmbH & Co.KGaA.: Weinheim* **2004**.

[59] Shaw, P. E.; Ruseckas, A.; Samuel, I. D. W. Exciton Diffusion Measurements in Poly(3-hexylthiophene). *Adv. Mater.* **2008**, *20*, 3516-3520.

[60] Zhang, F.; Jespersen, K. G.; Björström, C.; Svensson, M.; Andersson, M. R.; Sundström, V.; Magnusson, K.; Moons, E.; Yartsev, A.; Inganäs, O. Influence of Solvent Mixing on the Morphology and Performance of Solar Cells Based on Polyfluorene Copolymer/Fullerene Blends. *Adv. Funct. Mater.* **2006**, *16*, 667-674.

[61] Hwang, I. W.; Moses, D.; Heeger, A. J. Photoinduced Carrier Generation in P3HT/PCBM Bulk Heterojunction Materials. *J. Phys. Chem.C* **2008**, *112*, 4350-4354.

[62] Howard, I. A.; Mauer, R.; Meister, M.; Laquai, F. DFT Study of the Structure and Reactivity of the Terminal Pt(IV)-Oxo Complex Bearing No Electron-Withdrawing Ligands. *J. Am. Chem. Soc.* **2010**, *132*, 14866-14900.

[63] Holcombe, T. W.; Norton, J. E.; Rivnay, J.; Woo, C. H.; Goris, L.; Piliego, C.; Griffini, G.; Sellinger, A.; Bredas, J. L.; Salleo, A.; Frechet, J. M. J. Steric Control of the Donor/Acceptor Interface: Implications in Organic Photovoltaic Charge Generation. *J. Am. Chem. Soc.* **2011**, *133*, 12106-12114.

[64] Liu, T.; Cheung, D. L.; Troisi, A. Structural variability and dynamics of the P3HT/PCBM interface and its effects on the electronic structure and the charge-transfer rates in solar cells. *Phys. Chem. Chem. Phys.***2011**, *13*, 21461-21470.

[65] Arkhipov, V. I.; Heremans, P.; Bässler, H. Why is Exciton Dissociation So Efficient at the Interface between a Conjugated Polymer and an Electron Acceptor? *AIP*, **2003**; Vol. 82.

[66] Borsenberger, P. M.; Pautmeier, L.; Bässler, H. Charge Transport in Disordered Molecular Solids. *J. Chem. Phys.* **1991**, *94*, 5447-5454.

[67] Arkhipov, V. I.; Emelianova, E. V.; Bässler, H. Equilibrium Carrier Mobility in Disordered Hopping Systems. *Philosophical Magazine Part B* **2001**, *81*, 985-996.

[68] Bässler, H.; Borsenberger, P. M. The Transition from Nondispersive to Dispersive Charge Transport in Vapor Deposited Films of 1-phenyl-3-p-diethylamino-styryl-5-p-diethylphenylpyrazoline (DEASP). *Chem. Phys.* **1993**, *177*, 763-771.

[69] Juška, G.; Genevičius, K.; Nekrašas, N.; Sliaužys, G.; Österbacka, R. Two Dimensional Langevin Recombination in Regioregular Poly(3-hexylthiophene). *Appl. Phys. Lett.* **2009**, *95*, 013303.

[70] Valadares, M.; Silvestre, I.; Calado, H.; Neves, B.; Guimaraes, P.; Cury, L. BEHP-PPV and P3HT Blends for Light Emitting Devices. *Mater. Sci. Eng. C* **2009**, *29*, 571-574.

[71] Gburek, B.; Wagner, V. Influence of the Semiconductor Thickness on the Charge Carrier Mobility in P3HT Organic Field-effect Transistors in Top-gate Architecture on

Flexible Substrates. *Org. Electron.* **2010**, *11*, 814-819.

[72] Coakley, K. M.; McGehee, M. D. Photovoltaic Cells Made from Conjugated Polymers Infiltrated into Mesoporous Titania. *Appl. Phys. Lett.* **2003**, *83*, 3380-3382.

[73] Günes, S.; Sariciftci, N. S. Hybrid Solar Cells. *Inorg. Chim. Acta* **2008**, *361*, 581-588.

[74] Giulianini, M.; Waclawik, E. R.; Bell, J. M.; Scarselli, M.; Castrucci, P.; Crescenzi, M. D.; Motta, N. Poly(3-hexyl-thiophene) Coil-wrapped Single Wall Carbon Nanotube Investigated by Scanning Tunneling Spectroscopy. *Appl. Phys. Lett.* **2009**, *95*, 143116-143119.

[75] Ma, C. Y.; Gong, X.; Lee, K.; Heeger, A. Thermally Stable, Efficient Polymer Solar Cells with Nanoscale Control of the Interpenetrating Network Morphology. *Adv. Funct. Mater.* **2005**, *15*, 1617-1622.

[76] Liang, Y.; Xu, Z.; Xia, J.; Tsai, S. T.; Wu, Y.; Li, G.; Ray, C.; Yu, L. For the Bright Future-Bulk Heterojunction Polymer Solar Cells with Power Conversion Efficiency of 7.4%. *Adv. Mater.* **2010**, *22*, E135-138.

Chapter 2. Fabrication of sub-1D P3HT nanopillars array and the application in solar cell

According to the discussion in section 1.2.4 and 1.2.6, in the application of organic semiconductor in organic solar cells, the phase separation in nanoscale is essential. Thus formed interface is a postulate for exiction dissociation. Meanwhile, to ensure the exictons move to the formed interface in their lifetime and then the separated carriers transport to the electrodes, the separated phase domains should be confined in small enough scales and be continuous, namely, avoiding isolated domains. In this chapter, we established the formation of uniform sub-1D P3HT nanopillars *growing* on a continuous P3HT back film. By meaning of this, continuous P3HT phase was formed and the size of the formed pillars is tens of nanometers, close to the exciton diffusion length in polymer.

2.1 Introduction

Bulk heterojunction (BHJ) solar cells [1, 2] are superior to single- [3] and double-layer cells [4]. The BHJ structure can be formed simply by mixing a donor and acceptor solution. This straightforward technique is advantageous in terms of increasing the donor/acceptor (D/A) interface, which provides the exciton dissociation sites. Meanwhile, a weak point as regards BHJs is that the pathways of the generated carriers are not ensured because of the random phase separation of the respective materials. To ensure exciton dissociation and carrier collection, continuous percolation pathways are required.

An ideal structure would be an interdigitated interface, where the donor and acceptor phases are separate. The diameter and interspatial distance of the pillars should preferably be comparable to the diffusion length of the excitons, which is of the order of 10 nm. Then, the excitons can diffuse to the D/A interface during their lifetime [5]. Furthermore, the

interdigitated structure must be aligned perpendicularly to connect with the electrodes so as to provide direct pathways for efficient charge transportation [6, 7]. Meanwhile, the film thicknesses should be around 100 to 200 nm to absorb the incident light and to confine the series resistance [8, 9]. For these reasons, the dimensions of the interdigitated structures should be carefully designed to enhance photovoltaic effects. Interdigitated structures have been obtained using different techniques including self-organization and nanoimprinting [10, 11]. However, there is still room for further optimization of the dimensions [12].

2.2 Strategy of fabrication of sub-1D P3HT nanopillars and interdigitated solar cell

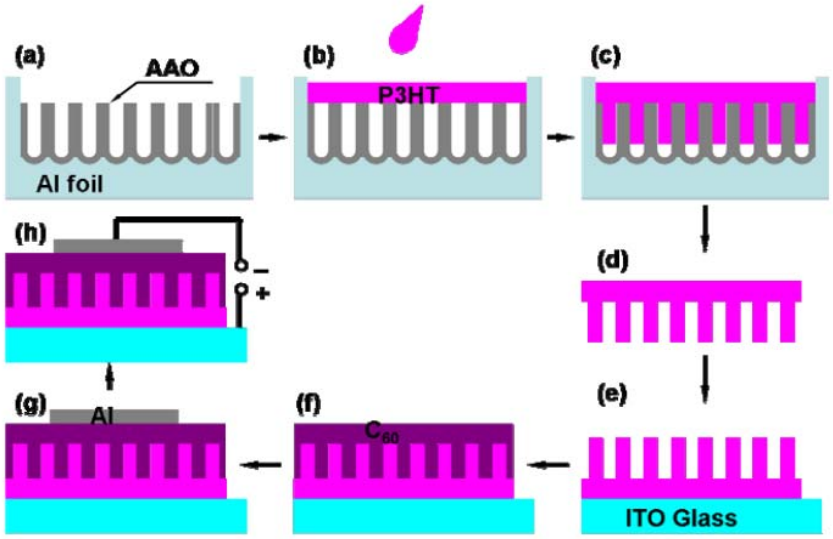

Figure 2-1 Polymer solar cell fabrication process. (**a**) AAO template. (**b**, **c**) Spin coating of P3HT solution and infiltration into pores. (**d**, **e**) Extraction of P3HT pillar film and transfer onto ITO substrate. (**f**, **g**) Vacuum deposition of C_{60} molecules and Al electrode. (**h**) *I-V* measurement.

In this chapter, we employed an anodic aluminum oxide (AAO) template to prepare a poly(3-hexylthiophene) (P3HT)/fullerene (C_{60}) interdigitated interface. P3HT absorbs the light from 400 to 700 nm to generate excitons. Meanwhile, C_{60} absorbs the light in the UV range of 300 to 400 nm and acts as an electron acceptor to transport such electrons to the electrode [9, 13]. The fabrication process and experimental procedures are schematic illustrated in Figure 2-1 and the detailed description will be shown in the experimental section. This strategy has the following merits: Firstly, the pillar size can be well controlled as regards diameter, interval, and height, making it close to the exciton diffusion length. Secondly, a carrier pathway can be formed, which is directly connected to the electrodes.

Finally, self-standing pillars can be fabricated uniformly over a large area. Besides, with this technology, costly imprinting equipment and cumbersome processes like dry etching [14, 15] are avoidable. By employing these advantages, we demonstrate the fine-tuning of nanostructures for organic solar cells and show preliminary device properties.

2.3 Information of main chemicals and equipment.

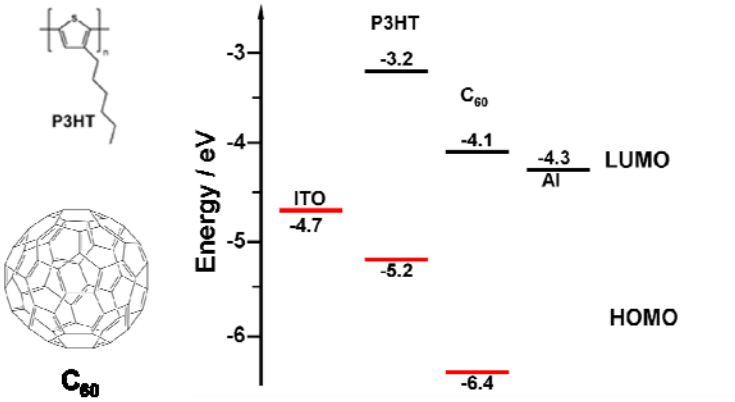

Figure 2-2. (a) Molecular structures of P3HT and C_{60}. (b) Schematic energy level diagram of each part of the fabricated cell.

P3HT and C_{60} are commercial available, the molecular structures of P3HT and C_{60} are shown in Figure 2-2. Also, the energy level of each part of the fabricated cell is illustrated, showing that each part involved in the formed device corresponds the fundamental mechanism of fabricating photovoltaic device according the discussion in section 1.2.3.

For deposition of C_{60}, a vacuum deposition system was employed. The main structure of the vacuum system is schematic illustrated in Figure 2-3. In this system, C_{60} located in a Knudsen Cell could be heated by the current of the outer surrounding resistance wire. Tuning the current, the temperature could be controlled. When the temperature is higher than gasification temperature (T_g), C_{60} irradiation occur and higher temperature leads to a higher irradiation rate. The irradiated C_{60} malecules thus deposits on the fronting samples which is connected on the sample holder. Importantly, the deposition rate is controllable by the heating temperature and deposition time could be controlled by opening and closing the shutter.

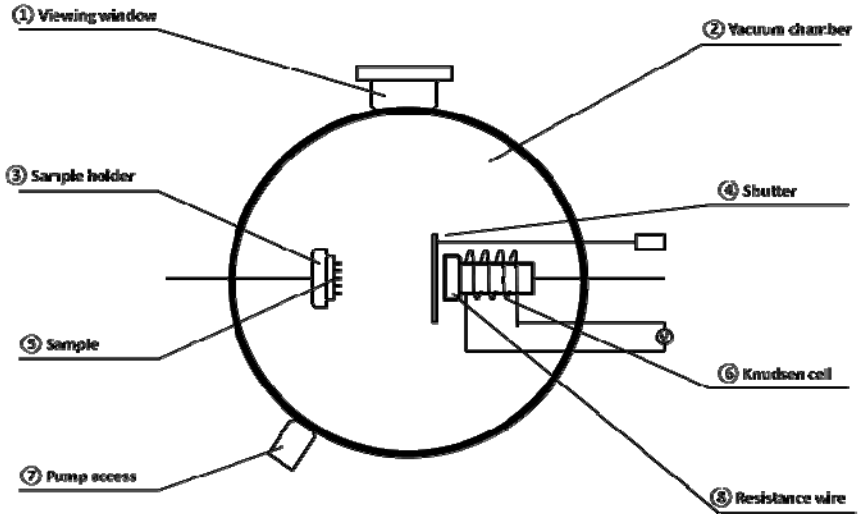

Figure 2-3. A illustration of the vacuum system for deposition of C_{60}. C_{60} molecules were placed in the Knudsen cell and the temperature and deposition rate can be controlled by tuning the current of the resistance wire.

2.4 Experimental details

2.4.1 General procedure for the preparation of AAO template

An AAO template was prepared by a conventional procedure using Al sheet (1 mm in thickness) with three main steps: first anodization, removal of the oxide layer, and second anodization [16]. For the first anodization, a constant voltage of 40 V was applied for 12 h in 0.3 M oxalic acid solution at 0°C. The alumina pores thus grown were etched away in a mixed solution of phosphoric acid (6% H_3PO_4) and chromic acid (1.8% CrO_3) for 12 h at 60°C. These procedures were needed to obtain a regular array of alumina dimples. The second anodization was initiated from these dimples and resulted in a highly ordered array of pores. The pore depth can be adjusted with the second anodization, which is performed under the same conditions as the first anodization. A subsequent widening process in 10% (*v*/*v*) phosphoric acid allowed fine-tuning of the pore diameters (Figure 2-1a).

2.4.2 Preparation of P3HT pillars standing on P3HT film

To prepare the P3HT nanopillars, a P3HT solution (3 wt.% in chlorobenzene) was spin coated on the AAO template at a rotation speed of 3,500 rpm (Figure 2-1b). The P3HT solution penetrated into the pores through capillary force to form P3HT nanopillars (Figure 2-1c) [17]. The alumina and Al substrate were removed by immersing the sample in 3 M NaOH solution for 45 min, and as a result, a self-standing P3HT film was obtained with a pillar structure on its surface (Figure 2-1d). Then, the P3HT film was soaked in a 3 M NaOH solution and rinsed in pure water to remove any remaining alumina particles and impurities.

2.4.3 Transfer pillars array contained P3HT film to ITO substrate

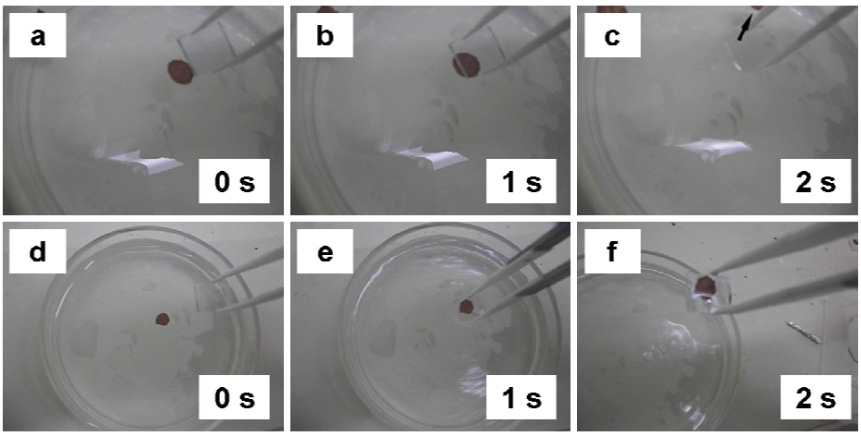

Figure 2-4 Comparison of ITO substrates before and after modification by chloroform. Before modification, when the ITO substrate approached the P3HT pillar film's reverse side (a, b), the film was pushed away (c). After modification, when the ITO substrate approached the P3HT pillar film's reverse side (d, e), the film was attached to the substrate (f).

To fabricate a photovoltaic device, the reverse side of the P3HT pillar film should be attached to an indium tin oxide (ITO) substrate. For this purpose, the surface tension of the ITO substrate was modified by soaking it in chloroform for 40 min [18]. The chloroform treatment increased the affinity of the ITO surface for the P3HT films and made it easier to attach them to the ITO substrates (Figure 2-1e, Figure 2-4).

2.4.4 Characterization method

Scanning electron microscope (SEM) images were obtained with an SU8000 Hitachi scanning electron microscope (Minato-ku, Japan). The *I-V* curve was measured with a WXS-90S-L2 super solar simulator (WACOM, Fukaya-shi, Japan; Figure 2-1h). All

measurements were performed under AM 1.5 irradiation (100 mW/cm^2) with a 0.04 cm^2 active surface area.

2.5 Results and discussion

2.5.1 Dimensional control of P3HT pillars by AAO template

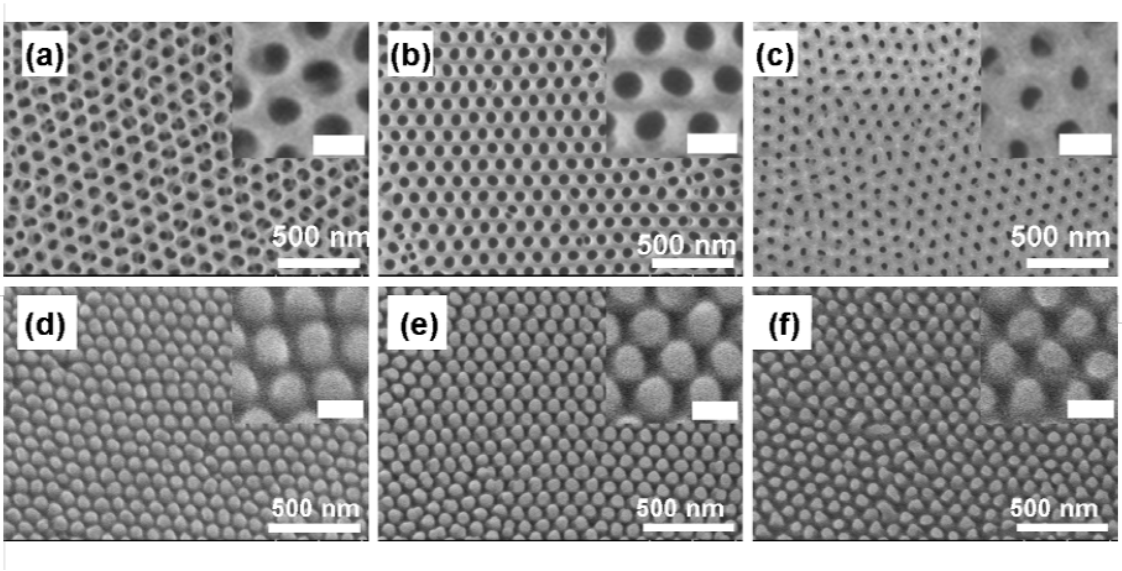

Figure 2-5 SEM images of AAO templates and PH3T nanopillars. (**a**, **b**, **c**) SEM images of AAO templates with different pore diameters of (a) 80, (b) 60, and (c) 40 nm. (**d**, **e**, **f**) SEM images of P3HT nanopillars with diameters of (d) 80, (e) 60, and (f) 40 nm. Samples (d, e, f) were tilted by 30°. The insets show enlarged images (bar length, 100 nm)

Figure 2-5a, b, c show SEM images of AAO templates. The diameters of the pores were tuned from 40 to 80 nm by adjusting the widening time from 1 to 10 min. The SEM images in Figure 2-5d, e, f show P3HT pillars. These images were obtained after removing the

AAO templates with NaOH solution. The diameters of the pillars ranged from 40 to 80 nm, and their intervals coincided well with those of the respective templates. In general, the diffusion length of the excitons in organic semiconductors is in the few tens-of-nanometer range. Therefore, the fine-tuning of the diameters of the pillars demonstrated here is advantageous for dimensional optimization in BHJ solar cells.

Importantly, the P3HT pillar heights were very uniform at about 100 nm regardless of diameter. The height should be optimized to maintain mechanical stability and to enhance light absorption. If the pillars are too tall, aggregation and collapse occur (Figure 2-6). Meanwhile, the pillars should be tall enough to promote light absorption. The height of 100 nm was optimized to satisfy these requirements by adjusting the second anodization time to 70 s. Pillar height uniformity is another essential factor as regards device operation. Such highly regulated P3TH pillars were observed over the template area. Consequently, the AAO template was shown to be a powerful technique for controlling the nanoscale dimensions of the P3HT pillars, namely diameter, interval, and height, as well as their uniformity over a wide area of about 100 mm^2.

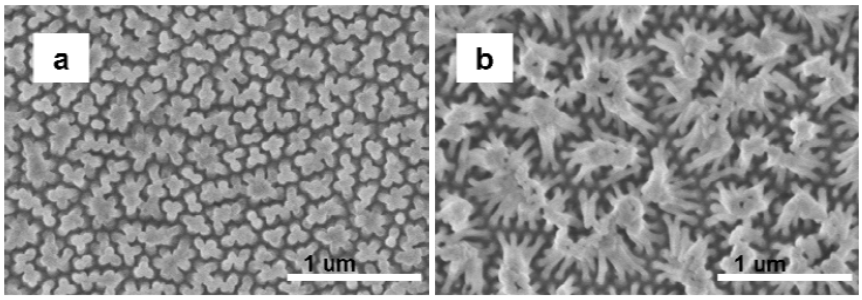

Figure 2-6 SEM images of P3HT nanowires fabricated by using AAO template prepared by controlling the second anodization time for (a) 2 and (b) 5 min.

2.5.2 Fabrication of P3HT/C_{60} interdigitated p-n heterojunction

C_{60} molecules were deposited on the P3HT pillar surface to form a interdigitated p-n junction in vacuum with a background pressure of 1×10^{-6} Pa (Figure 2-1f). The deposition rate was 10 to 20 nm/h, which was controlled by the temperature of a Knudsen cell. Then, a 120-nm-thick Al electrode was deposited on the C_{60} film (Figure 2-1g) in a thermal evaporation system. The P3HT/C_{60} p-n junction thus prepared was annealed in a vacuum at 180°C for 20 min. Figure 2-7a is a top-view SEM image of the C_{60} film on the P3HT pillars. A SEM image of the C_{60} film deposited on a flat glass substrate is shown in Figure 2-7b for comparison. Both images show a similar surface morphology; the C_{60} molecules aggregated to form a rough surface, but the entire surface was completely covered with a continuous film.

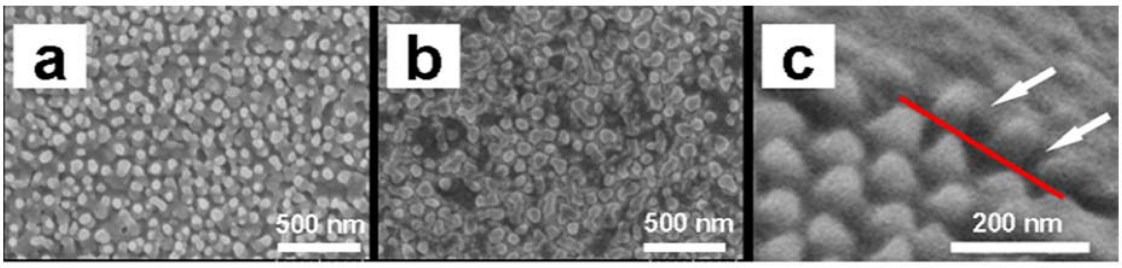

Figure 2-7. SEM images of deposited C_{60} films and P3HT/C_{60} heterojunction. SEM images of (a) C_{60} film deposited on P3HT pillars, (b) C_{60} film deposited on a flat substrate, and (c) cross section of P3HT/C_{60} heterojunction, proving full infiltration of C_{60} between P3HT pillars.

A major concern is the interfacial area between P3HT and C_{60}. The C_{60} molecules should be inserted between the P3HT pillars to form an interdigitated interface. To confirm the realization of such an embedded interface structure, a cross-sectional SEM image was obtained as shown in Figure 2-7c. For this sample, C_{60} molecules were deposited through a shadow mask. The image shows the border between the masked and unmasked areas (red line). The image clearly reveals that the deposited C_{60} molecules infiltrated between the

P3HT pillars as indicated by the arrows. After deposition of C_{60} molecules, the thickness of the heterojunction is controlled in a suitable scale (no more than 200 nm; Figure 2-8). The whole thickness consists of three parts: back film thickness, pillar height, and C_{60} film thickness. Thickness of the back film can be controlled by spin coating rate, pillar height can be controlled by AAO template pore depth, and deposition rate and time decide the C_{60} film thickness. After an Al cathode depositing on the C_{60} film to form a photovoltaic device, the specimen was thermally annealed to improve the ordering of the polymer chains and crystallinity [19].

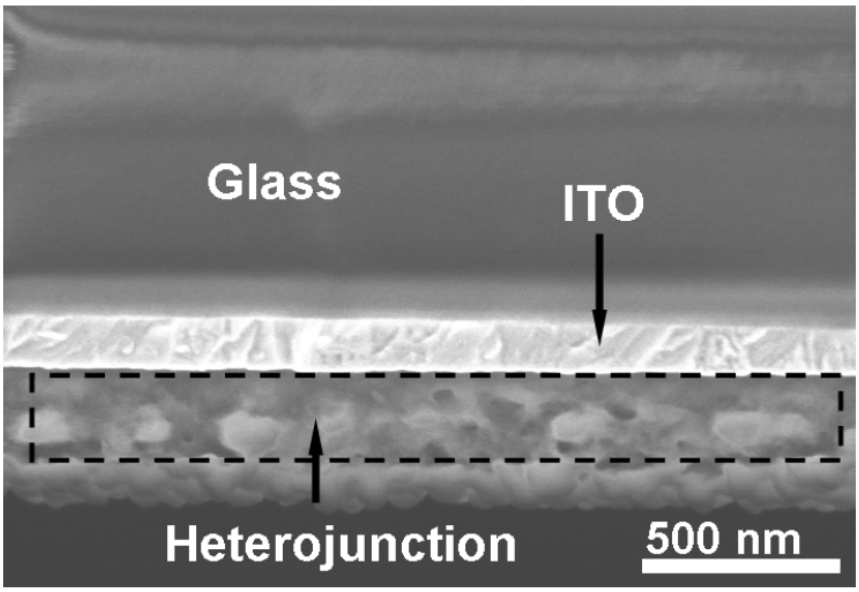

Figure 2-8. SEM image of P3HT/C_{60} heterojunction.

2.5.3 Photovoltaic properties of fabricated P3HT/C_{60} interdigitated p-n heterojunction and analysis of the preliminary result

Figure 2-9 shows the *I-V* curve of the thus prepared photovoltaic device. The diameter of the P3HT pillars was 80 nm for this measurement. The device properties are summarized in

the table in Figure 2-9. The poor performance is attributed to the sample preparation procedures, e.g., exposure to air during sample handling and transferring the film to ITO in water which may lead to a poor electrical contact. Also, during the removal of AAO template, there might be some impurity splashing to the reverse side of the P3HT pillar film because of the violent reaction, causing a contamination at the interface between ITO and P3HT. Nevertheless, this result demonstrates that the P3HT/C_{60} heterojunction produced by the AAO template can yield a photovoltaic effect.

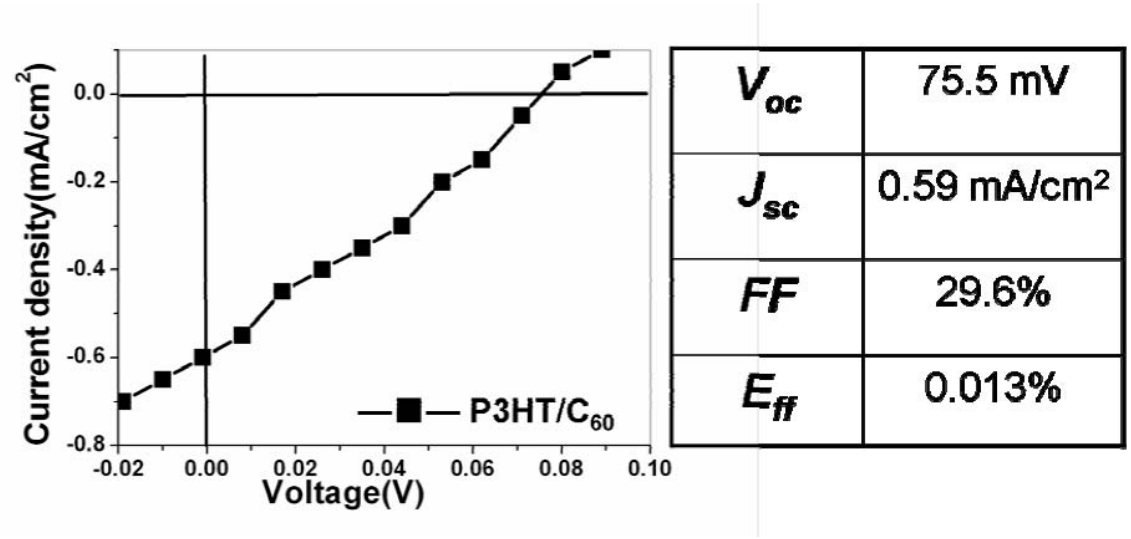

Figure 2-9. *I-V* curve of ITO/P3HT:C_{60}/Al organic photovoltage device. The properties are shown in the table. (nanopillar diameter, 80 nm)

2.6 Summary

In this chapter, we described an AAO template technique for fabricating regular arrays of P3HT pillars and interdigitated p-n junctions of P3HT/C_{60}. The formed P3HT/C_{60} junctions were used to fabricate photovoltaic device. The device properties in this study were preliminary, and there is still room for further improvement.

2.7 Motivations and significances of this work

Structure design in nanoscale for organic solar cell is very important for improving device performance. Phase separation and phase continuity ensure the exicton separation and transport. Domains for each phase should be close to exicton diffusion length. In this work, the feature of the technique is the high controllability of the nanoscale dimensions, such as the diameter, interval, height, and uniformity of the sub-1D P3HT pillars *growing* on a continuous P3HT back film. That is, these dimensions can be tailored to improve effective light absorption and carrier dissociation and transport. Afterwards, a interdigitated structure was formed by deposition of C_{60}. Meanwhile, the whole thickness of fabricated device could be controlled in suitable scale by meaning of controlling the pillar height and C_{60} deposition time. Besides, the technique we demonstrated here has great potential for use in developing a practical device because nanoscale structures can be fabricated in a large area exceeding 100 mm^2.

References

[1] Hall, J. J.; Walsh, C. A.; Greenham, N. C.; Marseglia, E. A.; Friend, R. H.; Moratti, S. C.; Holms, A. B. Efficient Photodiodes from Interpenetrating Polymer Networks. *Nature* **1995**, *376***,** 498-500.

[2] Mihailetchi, V. D.; Koster, L. J.; Hummelen, J. C.; Blom, P. W. Photocurrent Generation in Polymer-fullerene Bulk Heterojunctions. *Phys. Rev. Let.t* **2004**, *93*, 216601-216604.

[3] Kallmann, H.; Pope, M. Photovoltaic Effect in Organic Crystals. *J. Chem. Phys.* **1959**, *30*, 585-586.

[4] Tang, C. W. Two-layer Organic Photovoltaic Cell. *Appl. Phys. Lett.* **1986**, *48*, 183-185.

[5] Peumans, P.; Yakimov, A.; Forrest, S. R. Small Molecular Weight Organic Thin-film Photodetectors and Solar Cells. *J. Appl. Phys.* **2003**, *93*, 3693-3723.

[6] Coakley, K. M.; McGehee, M. D. Conjugated Polymer Photovoltaic Cells. *Chem. Mater.* **2004**, *16*, 4533-4542.

[7] Gunes, S.; Neugebauer, H.; Sariciftci, N. S. Conjugated Polymer-based Organic Solar Cells. *Chem. Rev.* **2007**, *107*, 1324-1338.

[8] Somani, P. R.; Somani, S. P.; Umeno, M. Toward Organic Thick Film Solar Cells: Three Dimensional Bulk Heterojunction Organic Thick Film Solar Cell Using Fullerene Single Crystal Nanorods. *Appl. Phys. Lett.* **2007**, *91*, 173503.

[9] Kim, M. S.; Kim, B. G.; Kim. J. Effective Variables to Control the Fill Factor of Organic Photovoltaic Cells. *ACS Appl. Mater. Interfaces* **2009**, *1*, 1264-1269.

[10] Chen, F. C.; Lin, Y. K.; Ko, C. J. Submicron-scale Manipulation of Phase Separation in Organic Solar Cells. *Appl. Phys. Lett.* **2008**, *92*, 023307-023309.

[11] Yang, Y.; Mielczarek, K.; Aryal, M.; Zakhidov, A.; Hu, W. Nanoimprinted Polymer Solar Cell. *ACS Nano* **2012**, *6*, 2877-2892.

[12] Avnon, E.; Yaacobi-Gross, N.; Ploshnik, E.; Shenhar, R.; Tessler, N. Low Cost, Nanometer Scale Nanoimprinting-application to Organic Solar Cells Optimization. *Org. Electron.* **2011**, *12*, 1241-1246.

[13] Scott, L. T.; Boorum, M. M.; McMahon, B. J.; Hagen, S.; Mack, J.; Blank, J.; Wegner, H.; Meijere, A. A Rational Chemical Synthesis of C_{60}. *Science* **2002**, *295*, 1500-1503.

[14] Aryal, M.; Buyukserin, F.; Mielczarek, K.; Zhao, X. M.; Gao, J. M.; Zakhidov, A.; Hu, W. Imprinted Large-scale High Density Polymer Nanopillars for Organic Solar Cells. *J. Vac. Sc.i Techno.l B* **2008**, *26*, 2562-2566.

[15] Aryal, M.; Trivedi, K.; Hu, W. Nano-confinement Induced Chain Alignment in Ordered P3HT Nanostructures Defined by Nanoimprint Lithography. *ACS Nano* **2009**, *3*, 3085-3090.

[16] Lei, Y.; Yang, S.; Wu, M.; Wilde, G. Surface Patterning Using Templates: Concept, Properties and Device Applications. *Chem. Soc. Rev.* **2011**, *40*, 1247-1258.

[17] Baek, S. J.; Park, J. B.; Lee, W.; Han, S. H.; Lee, J.; Lee, S. H. A Facile Method to Prepare Regioregular Poly(3-hexylthiophene) Nanorod Arrays Using Anodic Aluminium Oxide Templates and Capillary Force. *New J. Chem.* **2009**, *33*, 986-990.

[18] Xu, Z. Q.; Li, J.; Yang, J. P.; Cheng, P. P.; Zhao, J.; Lee, S. T.; Li, Y. Q.; Tang, J. X. Enhanced Performance in Polymer Photovoltaic Cells with Chloroform Treated Indium Tin Oxide Anode Modification. *Appl. Phys. Lett.* **2011**, *98*, 253303-253305.

[19] Zhokhavets, U.; Erb, T.; Hoppe, H.; Gobsch, G.; Sariciftci, N. S. Effect of Annealing of Poly(3-hexylthiophene)/fullerene Bulk Heterojunction Composites on Structural and Optical Properties. *Thin Solid Films* **2006**, *496*, 679-682.

Chapter 3. Fabrication of one-dimensional (1D) P3HT nanowires and the improvement of their electrical conductivities

In the applications of P3HT, especially in organic field effect transistors and organic photovoltaic devices, a bottleneck is to increase the conductivity. To improve the conductivity, decreasing resistivity, there is a consensus that two main aspects should be considered. One is improving polymer crystallinity, which could be achieved by controlling formation process, like controlling solvent evaporation rate, or introduing thermal annealing process to improve chain alignment. The other important approach is introducing dopant. In this aspect, polymer conductivity is sensitive to the doping level. High doping level leads to a higher conductivity. In this chapter, we fucous on enhancing the conductivity by employing dopant and increasing doping level in P3HT nanowires.

3.1 Introduction

Poly(3-hexylthiophene) (P3HT) is one of the most promising conjugated polymers because of its good solubility, environmental stability. Its field-effect mobility of 0.2 $cm^2V^{-1}s^{-1}$ is the highest reported for a polymer [1]. Such high mobility is caused by the formation of a lamellar structure by the self assembly of alkyl side chains [2]. The conductivity of this polymer depends on the head-tail (H-T) regioregularity of the chain; the higher the regioregularity, the higher is the conductivity [3]. Furthermore, the conductivity of the P3HT depends on processing condition, e.g., the solvent-cast samples have 1 order higher conductivity than the melt-cooled samples [3]. Again, the spin-coated samples have 2 orders higher conductivity than that of the solvent-cast film [4]. Since the discovery of highly-conducting polyacetylene, [5] it has been well known that chemical doping changes the electric conductivity of conjugated polymers by several orders of magnitude [6]. By using iodine (I_2) as dopant the conduction in P3HT films could be enhanced, but different

doping level should be performed by different techniques [7]. Furthermore, in regionrandom P3HT (RRa-P3HT) the doping level achieved was found be higher than that in regioregular P3HT (RR-P3HT), indicating that I_2 was absorbed more deeply into RRa-P3HT than RR-P3HT. But RR-P3HT is much more popular in most applications because its better electrical properties. However, for organic semiconducting devices molecular doping is preferable, since field-induced drift of the relative large-size charged molecular dopants can be suppressed. Recently, P3HT based OFETs doped with the strong acceptor 2,3,5,6-tetrafluoro-7,7,8,8-tetracyanoquinodimethane (F4-TCNQ) have been reported [8, 9], in which P3HT works as a hole transport material. Meanwhile, F4-TCNQ can function as acceptors that increase the hole density owing to the high electron affinity of cyano groups and fluorine atoms. In these applications, a challenging task is to achieve high doping and thus improve the conductivity of P3HT.

One-dimensional (1D) nanomaterials have been intensively studied because of their potential for use in future optoelectronic devices [10−12]. Molecular nanowires in particular have been applied to various functional devices including transistors [13, 14], sensors [15, 16], and photovoltaic devices [17, 18]. These nanowire devices have been developed by taking advantage of the characteristics of the 1D structure, namely, its flexibility, high crystallinity, and increased volume−surface ratio. In Chapter 2, we used anodized aluminum oxide (AAO) template to prepare sub-1D nanopillars. Actullay, the directed assembly method using AAO templates is a well-established technique for growing molecular nanowires [19−22]. A great advantage of the AAO template is that a large number of nanowires with a uniform diameter and length can be readily produced even for organic/inorganic hybrid materials [23, 24] and heterogeneous materials [25, 26].

3.2 Strategy of fabrication of 1D P3HT nanowires doped with F4-TCNQ in different doping level

In this chapter, we are aiming to enhance the electrical conductivity of P3HT. We employed AAO template to fabricate F4-TCNQ doped P3HT nanowires and controlled the dopant in different concentrations. It has beeb confirmed that the nanowire conductivity is

size-dependent on the wire diameter [22], because of the enhancement of conjugation length in the smaller diameter nanowires. Here, we demonstrate another merit of the AAO template with respect to the synthesis of molecular nanowires. The capillary force in the nanopores of the AAO template compels the chemical dopants to mix into the main matrix at a high doping level and enhanced the conductivity in the molecular nanowires. Such high conductivity is not achievable with the conventional two-dimensional (2D) thin film geometry due to dopant segregation. The fabrication process of F4-TCNQ doped P3HT nanowires is shown in Figure 3-1 and the details are described in experimental section.

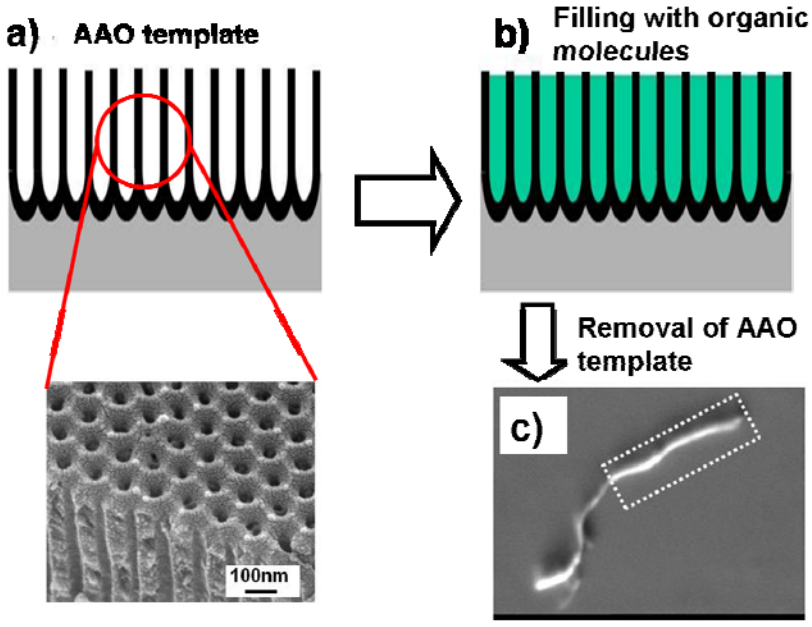

Figure 3-1. (a)-(c) Process of nanowire growth with AAO template. (c) shows a SEM image of a P3HT/F4-TCNQ composite nanowire on an SiO_2 (200 nm)/Si substrate. The straight and uniform part of the wire, indicated by a dotted line, was selected for the measurements. The inserted SEM image shows an anodized aluminum oxide template (cross section).

3.3 Informations of main chemicals and equipments

Regioregular poly(3-hexylthiophene) (P3HT) (purchased from Sigma-Aldrich and used as received; average number of thiophene monomers, 30 000−60 000; purity, 99.995%) and 2,3,5,6-tetrafluoro-7,7,8,8-tetracyanoquinodimethane (F4-TCNQ) (purchased from TCI and used as received; purity, 98%) were employed as the main matrix and chemical dopant, respectively. The molecular structures are shown in Figure 3-2.

To measure the resistivity in individual nanowires precisely, we employed a four-probe scanning tunneling microscope (STM), [27] which was integrated with a scanning electron microscope (SEM). With this technique, multiple measurements on nano-objects are available [28−30]. The movement of electrode could be manipulated and could be observed under the SEM system.

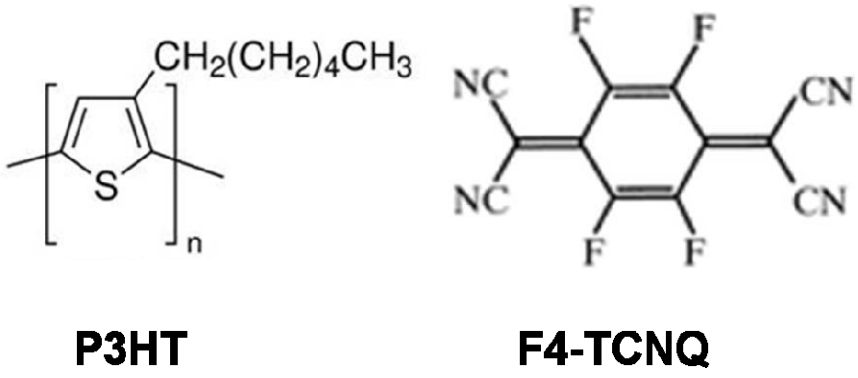

Figure 3-2. Molecular structures of P3HT and F4-TCNQ.

3.4 Experimental details of fabrication of F4-TCNQ doped P3HT nanowires and films, and the measurement methods

3.4.1 Fabrication of F4-TCNQ doped P3HT nanowires

The AAO templates with a pore size of about 80 nm were prepared by a conventional anodization process in oxalic acid [31] on 1-mm-thick Al sheets. The pore depth of the AAO template was about 24 μm, which was tuned by the anodization time of 3 h. The growth process of the P3HT/F4-TCNQ composite nanowires assisted by the AAO template is illustrated in Figure 3-1. First, P3HT and F4-TCNQ blended solutions with different concentrations, 0.1, 1.0, and 10 wt %, of F4-TCNQ were prepared in chlorobenzene. The solution was then dispersed on an AAO template. Second, the sample was introduced into a vacuum to anneal at 250 °C for 6 h. The molten P3HT/F4-TCNQ composite was introduced into the AAO nanochannels by capillary force. The sample was cooled gradually to solidify the P3HT/F4-TCNQ composite and form 1D nanowires. Third, the residual Al sheet on the back side was etched in $CuCl_2$ solution, and then the AAO templates were dissolved in NaOH solution to extract the P3HT/F4-TCNQ nanowires from templates. Ionic impurities such as Al^{3+}, Na^{+}, Cu^{2+}, and Cl^{-} must be thoroughly removed, particularly for reliable electrical measurements. For this purpose, the extracted nanowires were rinsed in pure water for 1 h. Finally, the nanowires thus prepared were dispersed on a highly doped Si substrate. The surface of the Si substrate was covered with a 200-nm-thick SiO_2 layer. The oxide thickness was selected to allow both stable SEM observation and the isolation of the nanowires from the Si substrate in the electrical measurement. The composite nanowire was curved because of its high aspect ratio and flexibility as shown in the SEM image. Only straight and uniform parts of the wires were measured with a four probe STM.

3.4.2 Fabrication of F4-TCNQ doped P3HT films

For comparison, the resistivities of P3HT/F4-TCNQ composite thin films were measured as references for those of nanowires. The F4-TCNQ concentrations of the mixed solution were the same as those for the nanowires: 0.1, 1.0 and 10.0 wt. %. The films were produced by spin coating on Si substrates, the surfaces of which were covered by SiO_2 layers to ensure insulating properties.

3.4.3 Electrical conductivity measurement of F4-TCNQ doped P3HT nanowires and films

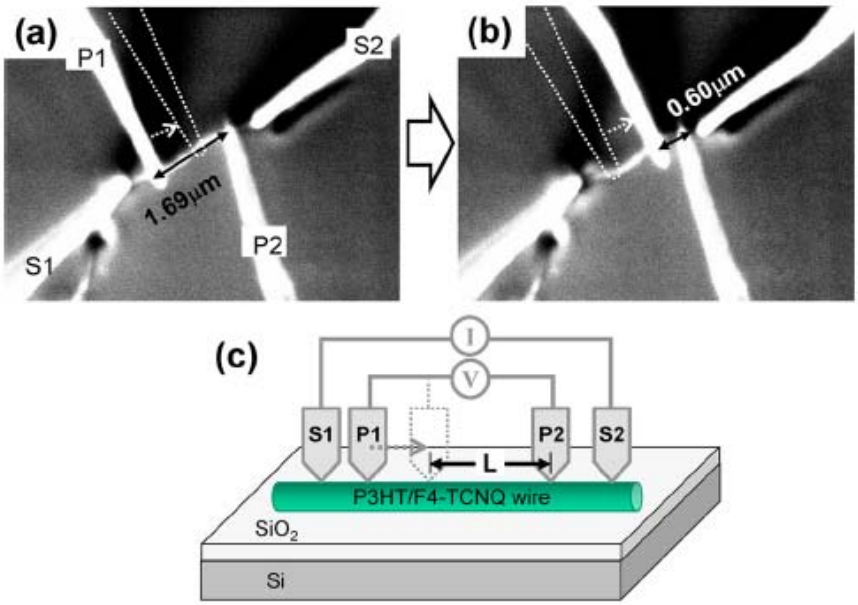

Figure 3-3. (a), (b) SEM images of the four-probe STM measurements. The outer pair of probes (S1 and S2) is fixed on both sides of the wire to provide electrical current. The inner pair (P1 and P2) monitors the voltage drop at each interval, where the position of P1 is varied from 1.69 to 0.60 μm, while P2 remains fixed at a certain position. (c) Schematic of the measurement procedure.

The transport measurements of P3HT/F4-TCNQ nanowires were performed in an ultrahigh vacuum chamber with a base pressure of less than 2×10^{-10} Torr. In this chamber, both SEM and STM are equipped to allow wide-area observation and local-area electric measurements. Various techniques have been utilized to measure nanowire resistivity, such as conductive atomic force microscopy [32, 33], focused ion beam electrode deposition [34, 35], and prepatterned electrodes [22, 36]. However, unstable electrical contacts between electrodes and nanowires have always been a concern in these measurements. In contrast,

the four-probe STM technique has significant benefits in providing stable contacts, suppressing the contact resistance effect, accessing individual measurement nano-objects, and especially in allowing multiple measurements on the same nanowires [28-30].On the basis of these considerations, we examined the electrical transport properties of molecular nanowires with a four-probe STM. Prior to the nanowire measurements, we confirmed that the leakage current through the substrate surface was negligible; ionic impurities were completely removed, and the oxide layer was thick enough to prevent unfavorable leakage.

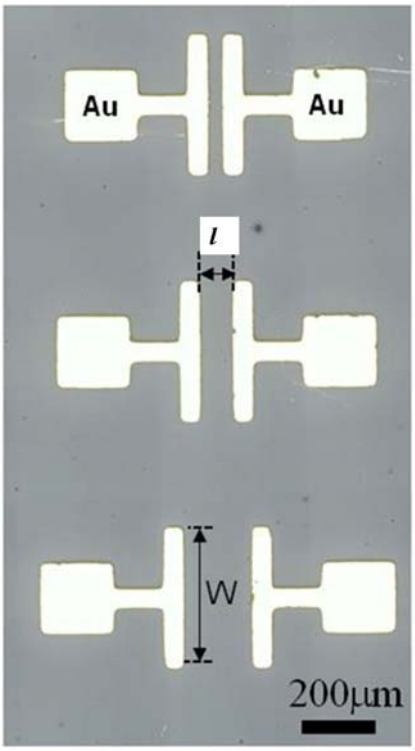

Figure 3-4. A photograph of the film sample. Electrodes with different intervals (*l*) were deposited on the same films simultaneously.

Under the guidance of an in situ SEM, all tungsten probes prepared by electrochemical etching were located precisely on the same nanowires. Reliable contact was verified by monitoring the stability of the electrical current flowing along the nanowire between any two probes. Source probes, denoted as S1 and S2 in Figure 3.3a, c, supplied the electrical

current using a Keithley 2400 source meter. The voltage drop was measured with another pair of probes (P1 and P2 in Figure 3-3a, c), which were connected to a Keithley 6430 voltage meter, to obtain the resistance at a specific probe spacing (L). Resistivity was determined by changing the intervals of the inner pair of probes, where one probe (P2) was placed at a fixed position while the contact position of the other probe (P1) moved along the wire as illustrated in Figure 3-3c. All measurements were carried out at room temperature.

The thicknesses of the respective films were measured with a contact probe thickness monitor. Au electrodes with different intervals (*l*) were deposited through shadow masks. The *l* values of the electrodes were varied from 50 to 200 μm to obtain resistance-interval lines. The electrode width (W) was 400 μm for all the electrodes. (Figure 3-4)

3.4.4 Absorption measurement of F4-TCNQ doped P3HT nanowires and films

Optical absorption spectra were measured with a UV−vis spectrophotometer (Jasco V-570) to examine the charge transfer and phase separation between P3HT and F4-TCNQ. Then, a template without wires was used as a reference for measuring the optical absorption of the nanowires in the template. The absorption spectra of the films were also obtained for comparison. The films were prepared on quartz substrates in a similar manner; the blended solution was spin coated on the substrate, followed by thermal annealing at 250 °C for 6 h in vacuum.

3.5 Results and discussion

3.5.1 Resistivity calculation of F4-TCNQ doped P3HT nanowires

The resistivity (ρ) of the nanowire was caculated with formula 3-1:

$$\rho = \frac{R}{L} S \tag{3-1}$$

where ρ, R, L and S represents nanowire resistivity, resistance, probe interval and cross section area of nanowire, respectively.

Figure 3-5 shows a resistance-interval plot of the composite nanowire with 10 wt % F4-TCNQ, obtained by changing the interval from 1.69 to 0.60 μm. The linear dependence indicates diffusive transport along the nanowire. The resistivity (ρ) of the nanowire was 0.16 Ωcm on the basis of the slope of the resistance−interval line (R/L) and the cross-section of the wire (S ≈ 5 × 10^3 nm^2). Similarly, the resistivities of the P3HT/F4- TCNQ composite nanowires with different F4-TCNQ concentrations are summarized in Table 3-1.

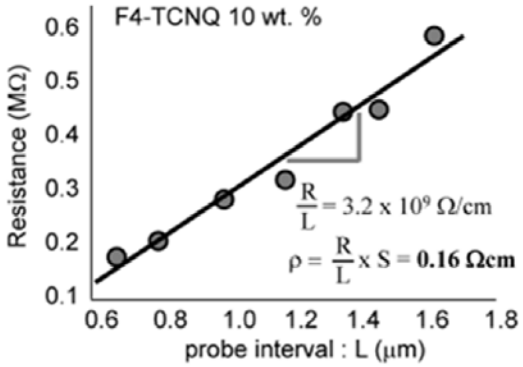

Figure 3-5. Interval-resistance line obtained from P3HT/F4-TCNQ nanowire with 10 wt. % of F4-TCNQ content. The slope of the line (R/L), together with the cross-section of the nanowire (S: ca. 5 × 10^3 nm^2) provide a resistivity (ρ).

Table 3-1. Resistance−interval slopes and resistivities of nanowires with different components.

F4-TCNQ Concentration	R/L (Ω/cm)	Resistivity (Ωcm)
0.1 wt.%	2.3 x 10^{11}	11.4
1 wt.%	6.1 x 10^9	0.30
10 wt.%	3.2 x 10^9	0.16

3.5.2 Resistivity calculation of F4-TCNQ doped P3HT films

For comparison, the resistivities of P3HT/F4-TCNQ composite films prepared by spin coating on the SiO_2/Si substrates were measured by using a two-terminal technique with Au electrodes. To eliminate the influence of contact resistance, the resistances (r) of the respective films were measured at different electrode intervals (l) from 50 to 200 μm, and the resistivity was estimated from the slope (r/l) of the resistance−interval plots and the film thicknesses (130−230 nm) based on formula 3-2:

$$\rho = \frac{r}{l} s \tag{3-2}$$

where s represents the cross section area of the tested film.

Measurement and calculation results of the samples with different doping concentration and same electrode interval (l = 200μm) are shown in Figure 3-6. Figure 3-6a shows the measured I-V curves of the samples and Figure 3-6b shows the caculated r/l slopes and resistivities based on the data from Figure 3-6a. The results are summarized in Table 3-2.

Table 3-2. Resistance−interval slopes and resistivities of films with different components.

F4-TCNQ Concentration	r/l (Ω/cm)	Resistivity (Ωcm)
0.1 wt.%	6.8×10^9	5.3×10^3
1 wt.%	6.3×10^9	5.1×10^3
10 wt.%	1.1×10^{10}	4.2×10^3

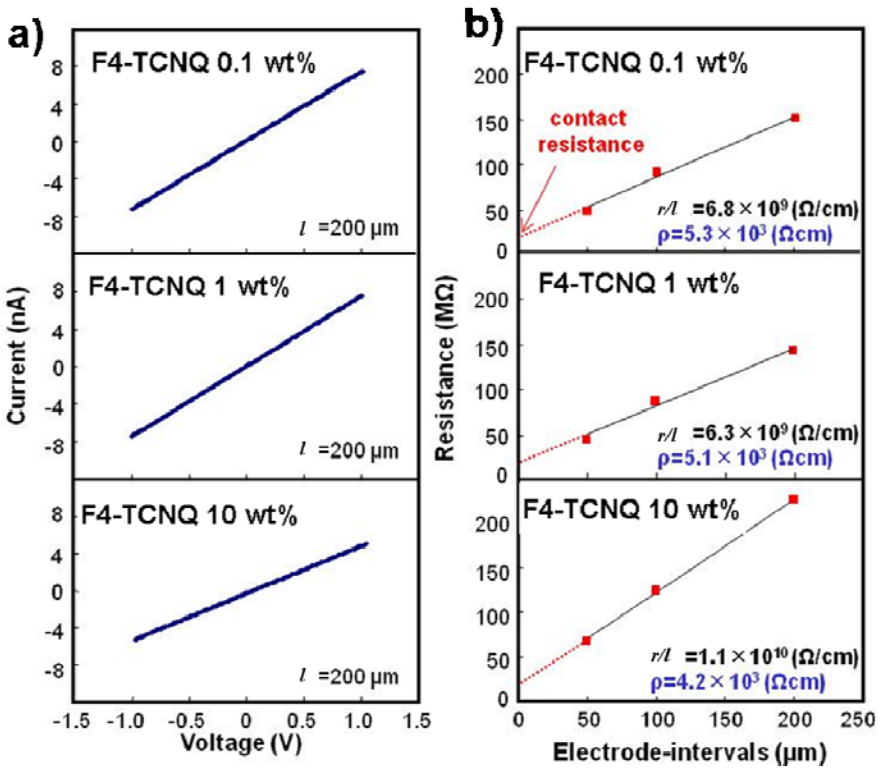

Figure 3-6. (a) shows the current-voltage (I-V) curves of the films. The observed straight lines confirmed ohmic contact between films and electrodes. (b) shows resistance-interval lines. The resistivities (ρ) were determined from the product of slopes (*r/l*), thicknesses and width (W).

3.5.3 Comparison of the resistivities of F4-TCNQ doped P3HT nanowires and films

The resistivities of doped nanowires decrease in proportion to the increase in the F4-TCNQ concentration in the 0.1−10 wt.% range (circle symbols in Figure 3-7). In general, P3HT acts as a p-type semiconductor, where holes are major carriers. Meanwhile, F4-TCNQ molecules work as acceptors because of the strong electron affinity of cyano groups and fluorine atoms. Therefore, the lowered resistivity can be attributed to the electron

transfer from P3HT to F4-TNCQ to increase the hole density in P3HT. We confirmed this tendency by repeating the same measurements three or four times for respective doping levels. Thus, the number of F4-TCNQ molecules that worked effectively as chemical dopants in P3HT was proportionally increased with increasing concentration over the entire doping range. As shown by the square symbols in Figure 3-7, the resistivities were around (4 to 5) × 10^3 Ωcm, almost independent of the F4-TCNQ concentration. Strikingly, the resistivity of the films was 2−4 orders of magnitude higher than that of the nanowires.

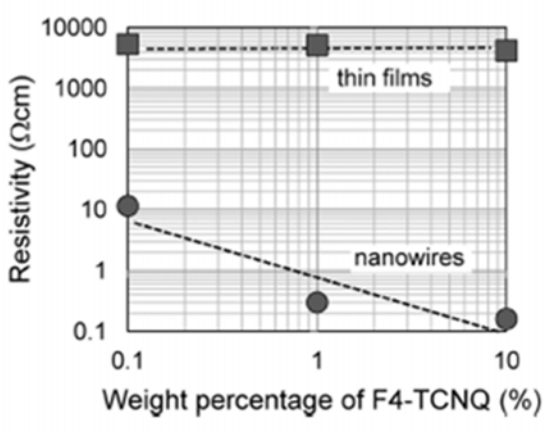

Figure 3-7. F4-TCNQ concentration dependence of resistivities for composite nanowires (circles) and thin films (squares).

3.5.4 Analysis of the influence of AAO template on the improvement of F4-TCNQ doped nanowires conductivities

The fact that the conductivity of the nanowires was better than that of the thin film can be attributed to two major effects introduced by using the AAO template. First, it has been reported that the nanoscale channels of an AAO template promote polymer chain alignment, and the resultant conductivity improvement is dependent on the diameter [37, 38]. It was indicated that a pore diameter of 80 nm can improve the conductivity of poly(3,4-ethylenedioxythiophene) nanowires by about 2 orders of magnitude [22]. Similar polymer

chain alignments induced by a nanospace confinement effect have been demonstrated using nanoimprint techniques [39−41]. Such polymer chain alignment has a great impact on carrier transport [2, 42], and Cui *et al.* reported a notable increase in the carrier mobility in a P3HT transistor realized with the nanoimprint technique [43]. In contrast, 0.2 wt % F4-TCNQ doping was reported to degrade the crystalline ordering of the P3HT thin films [8]. Thus, the lower resistivity of the nanowire with 0.1 wt % F4-TCNQ compared to that of the thin film can be ascribed to the improvement in the polymer alignment. However, the further improvement in the conductivity at a higher doping level cannot be explained simply by the polymer chain alignment. A second reason is the effective mixing of F4-TCNQ into P3HT in the AAO template.

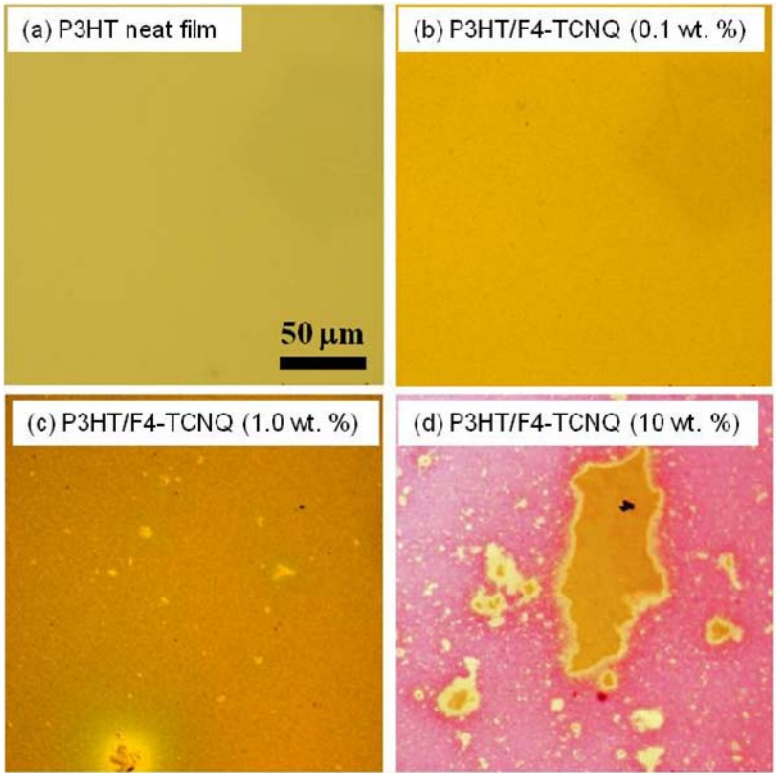

Figure 3-8. Optical microscope images of P3HT/F4-TCNQ composite films prepared by P3HT/F4-TCNQ solutions with F4-TCNQ concentration of (a) 0 wt.%, (b) 0.1 wt.%, (c) 1 wt.% and (d) 10 wt.%, respectively

In P3HT thin films, excess F4-TCNQ molecules can segregate (Figure 3-8). Film morphologies were observed for the neat P3HT and P3HT/F4-TCNQ composite films. All the films were prepared by spin coating in a similar manner to those used for the resistivity measurements. Figure 3-8(a)-(d) show optical microscope images of the surface morphologies of the respective films. Smooth and homogeneous surfaces were observed from (a) neat P3HT film and (b) P3HT with 0.1 wt. % composite film. Surface non-uniformity appeared from (c) 1.0 wt.% and became pronounced when the doping level was increased to (d) 10 wt. % as evidence of the phase separation between P3HT and F4-TCNQ. The inhomogeneous surface morphology of the film with the highest dopant concentration can be recognized even with the naked eye.

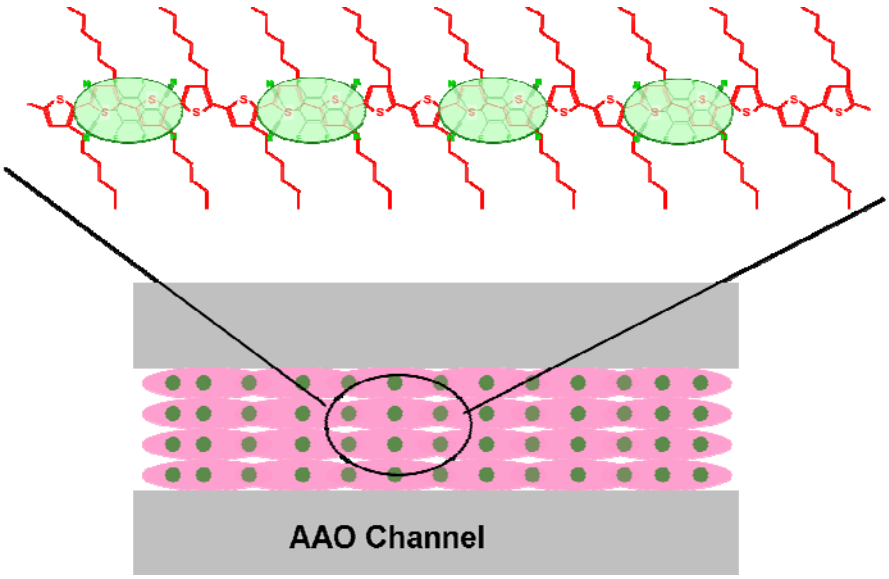

Figure 3-9. Illustration of F4-TCNQ doping in P3HT molecules in AAO channel forming doped P3HT/F4-TCNQ composite nanowire.

It has been reported that small molecules in a polymer matrix exhibit vertical phase separation [44] (i.e., the chemical doping concentration in the thin films has an upper limit). In fact, Zhang *et al.* reported that F4-TCNQ molecules segregated from P3HT to form a surface layer during the spin-coating process [28]. It is speculated that the F4-TCNQ

molecules are segregated in thin films and have no effect as a dopant, particularly at a high weight percentage. Consequently, a constant resistivity is observed in the thin films. In contrast, in the AAO template, the F4-TCNQ molecules are forced to mix into the P3HT matrix because of the capillary phenomenon in the AAO template. Figure 3-9 illustrates F4-TCNQ doping in P3HT nanowire in AAO channel.

The relationship of resistivity, carrier density and carrier mobility can be described as:

$$\rho = \frac{1}{pq\mu_p} \tag{3-3}$$

ρ: resistivity, p: hole density, q: electric quantity of hole (constant value), μ_p: carrier mobility.

In P3HT/F4-TCNQ system, the hole density p includes two part, the hole density of P3HT p_{P3HT} and hole density of F4-TCNQ p_{dopant}. So formula (3-3) can be described as:

$$\rho = \frac{1}{\left(p_{P3HT} + p_{dopant}\right)q\mu_p} \tag{3-4}$$

or

$$\rho = \frac{1}{\left(p_{P3HT} + D\chi\right)q\mu_p} \tag{3-5}$$

χ represents doping ratio, and D represents a slope parameter [45]. It has also been proved that a fraction of the applied F4-TCNQ dopants is active in creating free holes in polymer [46] and the ionized fraction increases with the increasing of doping ratio [47]. When the doping level increases over 1 wt.%, the distance between stacking layers along the alkyl chain reduces. Assuming that the charge transport is mainly controlled by the hopping process between the stacking layers, this results in the increase in mobility [48, 49]. Besides, the doped P3HT has increased conjugation length because of its higher crystalline order [50, 51]. These reasons cause the enhancement of carrier mobility μ_p. In our experiment, when the doping ratio increases from 0.1 wt.% to 10 wt.%, except the two orders of magnitude of

resisitivity decreased by the AAO channel, another 2 orders of magnitude should be introduced by doping effect. The concentration of dopant increased in two orders, but the hole density did not increase in 2 orders because of the presence of background hole density (p_{P3HT}) from P3HT. So the further decrease of resistivity is a combined action of hole density enhancement and carrier mobility enhancement.

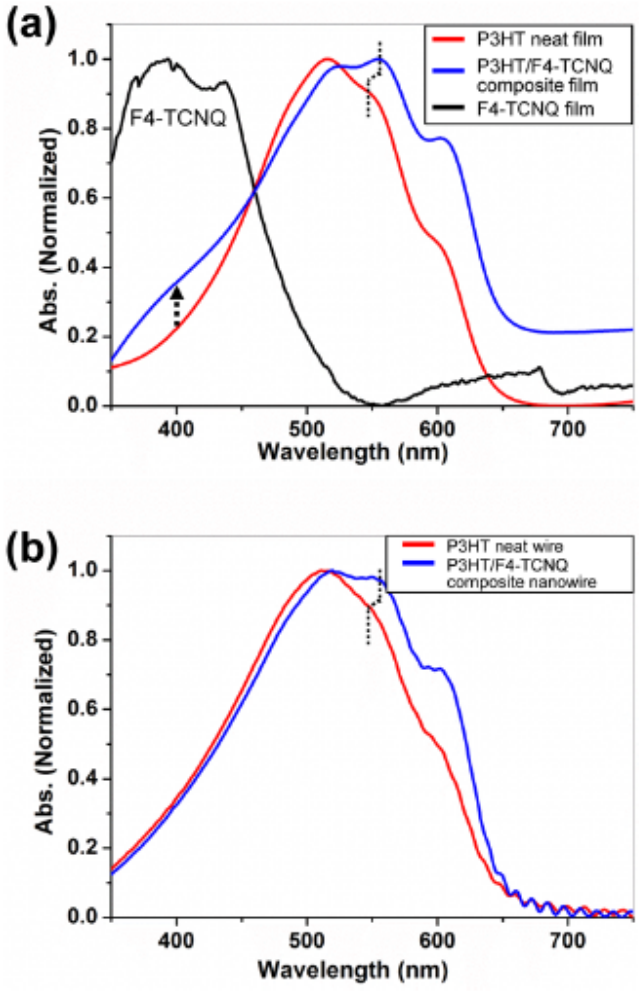

Figure 3-10. Absorption spectra of (a) neat P3HT film and P3HT/F4-TCNQ composite film, together with F4-TCNQ film, and (b) P3HT nanowires with and without F4-TCNQ dopants.

Absorption spectra were obtained to confirm the above discussion. Figure 5-10a shows absorption spectra from a neat P3HT film (red line) and a P3HT/F4-TCNQ (10 wt %) composite film (blue line). The absorption spectrum of an F4-TCNQ film (black line) is also shown for comparison. These spectra were normalized at the maximum peak. For the composite film, a peak shift from 540 to 550 nm was observed. This results from a charge transfer [8, 52] to extend the π conjugation. Another distinct variation induced by F4-TCNQ doping can be seen as an absorption increase from 350 to 450 nm, where the wavelength range coincides well with that of F4-TCNQ absorption (dotted arrow). This result suggests that F4-TCNQ molecules are segregated by phase separation. In contrast, no such increase in absorption was observed from the composite nanowire even at the same doping level, and the red shift at 550 nm was similarly observed as shown in Figure 3-10b. Namely, F4-TCNQ molecules were well mixed with P3HT, and no segregation occurred. These findings prove that the AAO technique is an effective approach to high-level doping. The improved alignment of the polymer chain together with the effective mixing of F4-TCNQ into P3HT in the AAO channels has led to better carrier conductivity in nanowires than in thin films.

The absorption of charge transfer over 1000 nm is not easy to observe because of two possible reasons: one is the aborption over 1000 nm is very weak comparing to the main absorption near 550 nm [53], the other one is the noise influence. In our experiment, when the wavelength exceeds 630 nm, the main signal is noise because of the complicated purify process of AAO template which may introduce impurities with immesurable amount. But it has been proved that F4-TCNQ molecules easily accept the electrons from P3HT backbones to form charge-transfer complexes and mobile carriers, which provides a strong electrostatic force between P3HT and F4-TCNQ molecules [8, 54-56].

3.6 Summary

We have demonstrated that P3HT/F4-TCNQ composite nanowires synthesized by employing an AAO template have superior conductivity comparing to thin films. A low resistivity of 0.16 Ω cm was achieved for the 10 wt % P3HT/F4-TCNQ composite nanowires, which was not possible with the thin film geometry.

3.7 Motivations and significances of this work

Improving conductivity, decreasing resistivity, is a bottleneck for the application of P3HT in electronic and optoelectronic devices. We used AAO template to improve the chain alignment of P3HT molecules and increase the dopant concentration, which meet the demands of conductivity improvement of conductive polymer. AAO template is a very powerful tool in this application because its channel have the small diameter to confine the molecular alignment and increase the conjugation length of P3HT molecules. By meanin of this, the P3HT molecule are arranged in higher crystalline order. Besides, capillary force in the nanoscale pores prevents the segregation of F4-TCNQ and enables high doping concentrations of up to 10 wt.% in P3HT.

Methodologically, to measure the resistivity in individual nanowires precisely, we employed a four-probe scanning tunneling microscope (STM), which was integrated with a scanning electron microscope (SEM). The four-probe STM technique has significant benefits in providing stable contacts, suppressing the contact resistance effect, accessing individual measurement nano-objects, and especially in allowing multiple measurements on the same nanowires.

References

[1] Wang, G. M.; Swensen, J.; Moses, D.; Heeger, A. J. Increased Mobility from Regioregular Poly(3-hexylthiophene) Field-effect Transistors. *J. Appl. Phys.* **2003**, *93*, 6137-6141.

[2] Sirringhaus, H.; Brown, P. J.; Friend, R. H.; Nielsen, M. M.; Bechgaard, K.; Langeveld-Voss, B. M. W.; Spiering, A. J. H.; Janssen, R. A. J.; Meijer, E. W.; Herwig, P.; de Leeuw, D. M. Two-Dimensional Charge Transport in Self-Organized, High-Mobility Conjugated Polymers. *Nature* **1999**, *401*, 685-688.

[3] Pal, S.; Roy, S.; Nandi, A. K. Temperature Variation of DC Conductivity of Poly(3-alkyl Thiophenes) and Their Cocrystals. *J. Phys. Chem. B* **2005**, *109*, 18332-18341.

[4] Kabashi, M.; Takeuchi, H. Inhomogeneity of Spin-Coated and Cast Non-Regioregular Poly(3-hexylthiophene) Films. Structures and Electrical and Photophysical Properties. *Macromolecules* **1998**, *31*, 7273-7278.

[5] Heeger, A. J.; Kivelson, S.; Schieffer, J. R.; Su. W.P. Solitons in Conducting Polymers *Rev. Mod. Phys.* **1988**, *60*, 781-850.

[6] Kaneko, H.; Ishiguro, T. Electrical Conductance in Metallic Phases of Fully Doped Polyacetylene. *Synth. Met.* **1994**, *65*, 141-148.

[7] Ukai, S.; Ito, H.; Marumoto, K.; Kuroda, S. I. Electrical Conduction of Regioregular and Regiorandom Poly(3-hexylthiophene) Doped with Iodine. *J. Phys. Soc. Jpn.* **2005**, *74*, 3314-3319.

[8] Ma, L.; Lee, W.-H.; Park, Y.-D.; Kim, J.-S.; Lee, H.-S.; Cho, K. High Performance Polythiophene Thin-Film Transistors Doped with Very Small Amounts of an Electron Acceptor. *Appl. Phys. Lett.* **2008**, *92*, 063310(1)-(3).

[9] Zhang, Y.; Blom, P. W. M. Enhancement of the Hole Injection into Regioregular Poly(3-Hexylthiophene) by Molecular Doping. *Appl. Phys. Lett.* **2010**, *97*, 083303-083305.

[10] Thelander, C.; Agarwal, P.; Brongersma, S.; Eymery, J.; Feiner, L. F.; Forchel, A.; Scheffler, M.; Riess, W.; Ohlsson, B. J.; Gösele, U.; Samuelson, L. Nanowire-Based One-Dimensional Electronics. *Mater. Today* **2006**, *9*, 28-35.

[11] Briseno, A. L.; Mannsfeld, S. C. B.; Jenekhe, S. A.; Bao, Z.; Xia, Y. Introducing Organic Nanowire Transistors. *Mater. Today* **2008**, *11*, 38-47.

[12] Coskun, A.; Spruell, J. M.; Barin, G.; Dichtel, W. R.; Flood, A. H.; Botrosgh, Y. Y.; Stoddart, J. F. High hopes: Can Molecular Electronics Realise Its Potential? *Chem. Soc. Rev.* **2012**, *41*, 4827–4859.

[13] Wakayama, Y.; Hayakawa, R.; Chikyow, T.; Machida, S.; Nakayama, T.; Egger, S.; G. de Oteyza, D.; Dosch, H.; Kobayashi, K. Self-Assembled Molecular Nanowires of 6,13-Bis(methylthio)pentacene: Growth, Electrical Properties, and Applications. *Nano Lett*. **2008**, *8*, 3273-3277.

[14] Briseno, A. L.; Mannsfeld, S. C. B.; Lu, X.; Xiong, Y.; Jenekhe, S. A.; Bao, Z.; Xia, Y. Fabrication of Field-Effect Transistors from Hexathiapentacene Single-Crystal Nanowires. *Nano Lett.* **2007**, *7*, 668-675.

[15] Hangarter, C. M.; Bangar, M.; Mulchandani, A.; Myung, N. V. Conducting Polymer Nanowires for Chemiresistive and FET-based Bio/Chemical Sensors. *J. Mater. Chem.* **2010**, *20*, 3131-3140.

[16] Shirsat, M. D.; Bangar, M. A.; Deshusses, M. A.; Myung, N. V.; Mulchandani, A. Polyaniline Nanowires-Gold Nanoparticles Hybrid Network Based Chemiresistive Hydrogen Sulfide Sensor. *Appl. Phys. Lett.* **2009**, *94*, 083502(1)-(3).

[17] Kim, K.; Lee, J. W.; Lee, S. H.; Lee, Y. B.; Cho, E. H.; Noh, H. S.; Jo, S. G.; Joo, J. Nanoscale Optical and Photoresponsive Electrical Properties of P3HT and PCBM Composite Nanowires. *Org. Electron.* **2011**, *12*, 1695-1700.

[18] Foong, T. R. B.; Chan, K.-L.; Hu, X. Structure and Properties of Nano-confined Poly(3-hexylthiophene) in Nano-array/Polymer Hybrid Ordered-bulk Heterojunction Solar Cells. *Nanoscale*. **2012**, *4*, 478-485.

[19] Joo, J.; Park, K.-T.; Kim, B.-H.; Kim, M.-S.; Lee, S.-Y.; Jeong, C.-K.; Lee, J.-K.; Park, D.-H.; Yi, W.-K.; Lee, S.-H.; Ryu, K.-S. Conducting Polymer Nanotube and Nanowire

Synthesized by Using Nanoporous Template: Synthesis, Characteristics, and Applications. *Synth. Met.* **2003**, *135-136*, 7-9.

[20] Braunschweig, A. B.; Schmucker, A. L.; Wei, W. D.; Mirkin, C. A. Nanostructures Enabled by On-Wire Lithography (OWL). *Chem. Phys. Lett.* **2010**, *486*, 89-98.

[21] Rabih, O. A.; Dillon, J. R.; Kaiser, J. M.; Mueller, L. J.; Guirado, G.; Bardeen, C. J. Photopolymerization of Organic Molecular Crystal Nanorods. *Macromolecules* **2007**, *40*, 9040-9044.

[22] Shirai, Y.; Takami, S.; Lasmono, S.; Iwai, H.; Chikyow, T.; Wakayama, Y. Improvement in Carrier Mobility of Poly(3,4-Ethylenedioxythiophene) Nanowires Synthesized in Porous Alumina Templates. *J. Polymer Sci. B: Polymer Phys.* **2011**, *49*, 1762-1768.

[23] Lee, J.; Jho, J. Y. Fabrication of Highly Ordered and Vertically Oriented TiO_2 Nanotube Arrays for Ordered Heterojunction Polymer/Inorganic Hybrid Solar Cell. *Solar Energy Materials and Solar Cells* **2011**, *95*, 3152-3156.

[24] Xiong, S. X.; Wang, Q.; Chen, Y. H. Preparation of Polyaniline/TiO_2 Hybrid Microwires in the Microchannels of a Template. *Mater. Chem. Phys.* **2007**, *103*, 450-455.

[25] Han, F. M.; Meng, G. W.; Zhao, X. L.; Xu, Q. L.; Liu, J. X.; Chen, B. S.; Zhu, X. G.; Kong, M. G. Building Desired Heterojunctions of Semiconductor CdS Nanowire and Carbon Nanotube via AAO Template-Based Approach. *Mater. Lett.* **2009**, *63*, 2249-2252.

[26] Liang, C.; Terabe, K.; Tsuruoka, T.; Osada, M .; Hasegawa, T .; Aono, M. AgI/Ag Heterojunction Nanowires: Facile Electrochemical Synthesis, Photoluminescence, and Enhanced Ionic Conductivity. *Adv. Func. Mater.* **2007**, *17*, 1466-1472.

[27] Kim, T.-H.; Zhang, X.-G.; Nicholson, D. M.; Evans, B. M.; Kulkarni, N. S.; Radhakrishnan, B.; Kenik, E. A.; Li, A.-P. Large Discrete Resistance Jump at Grain Boundary in Copper Nanowire. *Nano Lett.* **2010**, *10*, 3096-3100.

[28] Kaspers, M. R.; Bernhart, A. M.; Meyer zu Heringdorf1, F.-J.; Dumpich, G.; Möller, R. Electromigration and Potentiometry Measurements of Single-Crystalline Ag Nanowires under UHV Conditions. *J. Phys.: Condens. Matter.* **2009**, *212*, 65601-65606.

[29] Walton, A. S.; Allen, C. S.; Critchley, K.; Górzny, M. Ł.; McKendry, J. E.; Brydson, R. M. D.; Hickey, B. J.; Evans, S. D. Four-Probe Electrical Transport Measurements on Individual Metallic Nanowires. *Nanotechnology* **2007**, *18*, 065204-065210.

[30] Kim, T.-H.; Wendelken, J. F.; Li, A.-P.; Du, G.; Li, W. Probing Electrical Transport in Individual Carbon Nanotubes and Junctions. *Nanotechnology* **2008**, *19*, 485201-485206.

[31] van Dyke, L. S.; Martin, C. R. Fibrillar Electronically Conductive Polymers Show Enhanced Rates of Charge Transport. *Synth. Met.* **1990**, *36*, 275-281.

[32] Cao, H.; Wang, L.; Qiu, Y.; Zhang, L. Synthesis and *I–V* Properties of Aligned Copper Nanowires. *Nanotechnology* **2006**, *17*, 1736-1739.

[33] Weber, S. A. L.; Haberkorn, N.; Theato, P.; Berger, R. Mapping of Local Conductivity Variations on Fragile Nanopillar Arrays by Scanning Conductive Torsion Mode Microscopy. *Nano Lett*. **2010**, *10*, 1194-1197.

[34] Long, Y. Z.; Duvail, J. L.; Li, M. M.; Gu, C.; Liu, Z.; Ringer, S. P. Electrical Conductivity Studies on Individual Conjugated Polymer Nanowires: Two-Probe and Four-Probe Results. *Nanoscale Res. Lett.* **2010**, *5*, 237-242.

[35] Hernandez-Ramirez, F.; Tarancon, A.; Casals, O.; Pellicer, E.; Rodriguez, J.; Romano-Rodriguez, A.; Morante, J. R.; Barth, S.; Mathur, S. Electrical Properties of Individual Tin Oxide Nanowires Contacted to Platinum Electrodes. *Phys. Rev. B* **2007**, *76*, 085429(1)-(5).

[36] Boote, J. J.; Evans, S. D. Dielectrophoretic Manipulation and Electrical Characterization of Gold Nanowires. *Nanotechnology* **2005**, *16*, 1500-1505.

[37] Lei, Y.; Cai, W.; Wilde, G. Highly Ordered Nanostructures with Tunable Size, Shape Andproperties: A New Way to Surface Nano-Patterning Using Ultra-Thin Alumina Masks. *Progr. Mater. Sci.* **2007**, *52*, 465-539.

[38] Penner, R. M.; Martin, C. R. Controlling the Morphology of Electronically Conductive Polymers. *J. Electrochem. Soc*. **1986**, *133*, 2206-2207.

[39] Zheng, Z.; Yim, K.-H.; Saifullah, S. M. M.; Welland, E. M.; Friend, H. R.; Kim, J.-S.; Huck, T. S. W. Uniaxial Alignment of Liquid-Crystalline Conjugated Polymers by Nanoconfinement. *Nano Lett.* **2007**, *7*, 987-992.

[40] Aryal, M.; Trivedi, K.; Hu, W. Nano-Confinement Induced Chain Alignment in Ordered P3HT Nanostructures Defined by Nanoimprint Lithography. *ACS Nano* **2009**, *3*, 3085-3090.

[41] Hlaing, H.; Lu, X.; Hofmann, T.; Yager, G. K.; Black, T. C.; Ocko, M. B. Nanoimprint-induced Molecular Orientation in Semiconducting Polymer Nanostructures. *ACS Nano* **2011**, *5*, 7532-7538.

[42] Sirringhaus, H.; Wilson, R. J.; Friend, R. H.; Inbasekaran, M.;Wu, W.; Woo, E. P.; Grell, M.; Bradley, D. D. C. Mobility Enhancement in Conjugated Polymer Field-Effect Transistors Throughchain Alignment in a Liquid-Crystalline Phase. *Appl. Phys. Lett.* **2000**, *77*, 406–408.

[43] Cui, D.; Li, H.; Park, H.; Cheng, X. Improving Organic Thin-Film Transistor Performance by Nanoimprint-Induced Chain Ordering. *J. Vac. Sci. Technol. B*, **2008**, *26*, 2404-2409.

[44] Hamilton, R.; Smith, J.; Ogier, S.; Heeney, M.; Anthony, J. E.; McCulloch, I.; Veres, J.; Bradley, D. D. C.; Anthopoulos, T. D. High-Performance Polymer-Small Molecule Blend Organic Transistors. *Adv. Mat.* **2009**, *21*, 1166-1171.

[45] Pingel, P.; Schwarzl, R.; Neher, D. Effect of Molecular p-doping on Hole Density and Mobility in Poly(3-hexylthiophene). *Appl. Phys. Lett.* **2012**, *100*, 143303.

[46] Zhang, Y.; de Boer, B.; Blom, P. W. M. Controllable Molecular Doping and Charge Transport in Solution-Processed Polymer Semiconducting Layers. *Adv. Funct. Mater.* **2009**, *19*, 1901-1905.

[47] Pingel, P.; Neher, D. Comprehensive Picture of p-type Doping of P3HT with the Molecular Acceptor F4TCNQ. *Phys. Rev. B* **2013**, *87*, 115209.

[48] Winokur, M. J.; Wamsley, P.; Moulton, J.; Smith, P.; Heeger, A. J. Structural Evolution in Iodine-doped Poly(3-alkylthiophenes). *Macromolecules*, **1991**, *24*, 3812-3815.

[49] Jiang, X.; Harima, Y.; Yamashita, K.; Tada, Y.; Ohshita, J.; Kunai, A. Doping-induced Change of Carrier Mobilities in Poly(3-hexylthiophene) Films with Different Stacking Structures. *Chem. Phys. Lett.* **2002**, *364*, 616-620.

[50] Sandberg, H. G. O.; Frey, G. L.; Shkunov, M. N.; Sirringhaus, H.; Friend, R. H. Ultrathin Regioregular Poly(3-hexyl thiophene) Field-Effect Transistors. *Langmuir*, **2002**, *18*, 10176-10182.

[51] Zen, A.; Saphiannikova, M.; Neher, D.; Asawapirom, U.; Scherf, U. Comparative Study of the Field-Effect Mobility of a Copolymer and a Binary Blend Based on Poly(3-alkylthiophene)s. *Chem. Mater.*, **2005**, *17*, 781-786.

[52] Panda, P.; Veldman, D.; Sweelssen, J.; Bastiaansen, Jolanda J. A. M.; M. W. Langeveld-Voss, B.; Meskers, C. J. S. Charge Transfer Absorption for Conjugated Polymers and Oligomers Mixed with Electron Acceptors. *J. Phys. Chem. B*, **2007**, *111*, 5076-5081.

[53] Swensen, J. S.; Wang, L.; Rainbolt, J. E.; Koech, P. K.; Polikarpov, E.; Gaspar, D. J.; Padmaperuma, A. B. Characterization of Solution Processed, p-doped Films Using Hole-only Devices and Organic Field-effect Transistors. *Org. Electron.* **2012**, *13*, 3085-3090.

[54] Aziz, E. F.; Vollmer, A.; Eisebitt, S.; Eberhardt, W.; Pingel, P.; Neher, D.; Koch, N. Localized Charge Transfer in a Molecularly Doped Conducting Polymer. *Adv. Mater.* **2007**, *19*, 3257-3260.

[55] Bryce, M. R.; Murphy, L. C. Organic Metals. *Nature* **1984***, 309*, 119-126.

[56] Hotta, S.; Waragai, K. Alkyl-substituted Oligothiophenes: Crystallographic and Spectroscopic Studies of Neutral and Doped Forms. *J. Mater. Chem.* **1991**, *1*, 835-842.

Chapter 4. Fabrication of two-dimensional (2D) P3HT:PCBM films and the application in organic solar cell

Organic photovoltaic (OPV) device is a important application for P3HT. For the further development of OPV devices, on one hand, nanostructure design based on the electrical and photoelectric mechanism is essential to improve device performances (like the work described in Chapter 2), on the other hand, developing easy fabrication technique to lower cost should also be paid more attention to. Besides, enlarging the device area is an other consideration. Polymer bulk heterojunction (BHJ) is so far the most reliable structure for organic solar cells. Several techniques were proposed to make this kind of devices, but there are still blind angle for them. In this chapter, we proposed a new technique to fabricate a 2D P3HT film in a very easy way and tried to use the formed film as a OPV device.

4.1 Introduction

Organic solar cells, especially polymer bulk heterojunction (BHJ) solar cells, have attracted great interest during the past decade because of their potential to provide low cost, lightweight and flexible devices over a large area [1-3]. In BHJ solar cells, interpenetrating donor and acceptor networks result in efficient photo-induced charge separation. The device efficiency has exceeded 7% through the use of developed materials [4, 5]. As the next step, crucial requirements for practical applications include developing effective solution processes to reduce manufacturing costs and achieving a stable increase in efficiency.

The spin coating method has been established as the most reliable and reproducible process in research on high-efficiency polymer solar cells (PSCs) using the solution process

[6]. However, several problems including the production of a large amount of waste material, are unavoidable. Moreover, this method is only suitable for a limited substrate size. To achieve low-cost production and commercialization, we need a continuous process with a high throughput if we are to better utilize the great advantages of PSCs, especially when used on large area flexible substrates. Many deposition techniques have been demonstrated for PSC fabrication including ink-jet printing [7, 8], spray coating [9-11], and screen printing [12-14]. Each method has advantages over the spin coating method, but all these techniques require costly equipment. In contrast, the dip coating technique [15,16] has been developed as a cost effective method but it cannot be applied to soft substrates because organic solvent may dissolve the plastic substrate during solution processes. Therefore, there is an urgent need to develop a technique for fabricating large-scale PSCs at low cost with inexpensive equipment and little material waste. Moreover, the improved technique should be easily applicable to soft substrates such as polyethylene terephthalate (PET).

4.2 Strategy of fabrication of 2D ITO/PEDOT:PSS/P3HT:PCBM structure in a large scale

In this chapter, we describe a one-step fabrication technique for large-scale indium tin oxide/poly(3,4-ethylenedioxythiophene):poly(styrenesulfonate)/ poly(3-hexylthiophene-2,5-diyl):[6,6]-phenyl-C61-butyric acid methyl ester (ITO/ PEDOT:PSS/P3HT:PCBM) multi-layered structures that uses a solution process. The process is illustrated in Figure 4-1: ITO/Glass (or PET) substrate was sinked in PEDOT:PSS solution (Step 1) on which P3HT:PCBM solution was droped (Step 2). P3HT:PCBM solution spread immediately and subsequently fabricated a floating film after the solvent evaporation. Substrate was picked up from PEDOT:PSS solution, covering with the floated P3HT:PCBM film. PEDOT:PSS solution played as a media to adhere the substrate and the floating film. After drying, the ITO/PEDOT:PSS/PCBM:P3HT structure was obtained (Step 3). The sample was then dried and an ITO/PEDOT:PSS/PCBM:P3HT structure was obtained. The photo shows a

P3HT:PCBM film floating on PEDOT:PSS solution, marked by a dotted circle. We show that this process is achievable under very simple conditions.

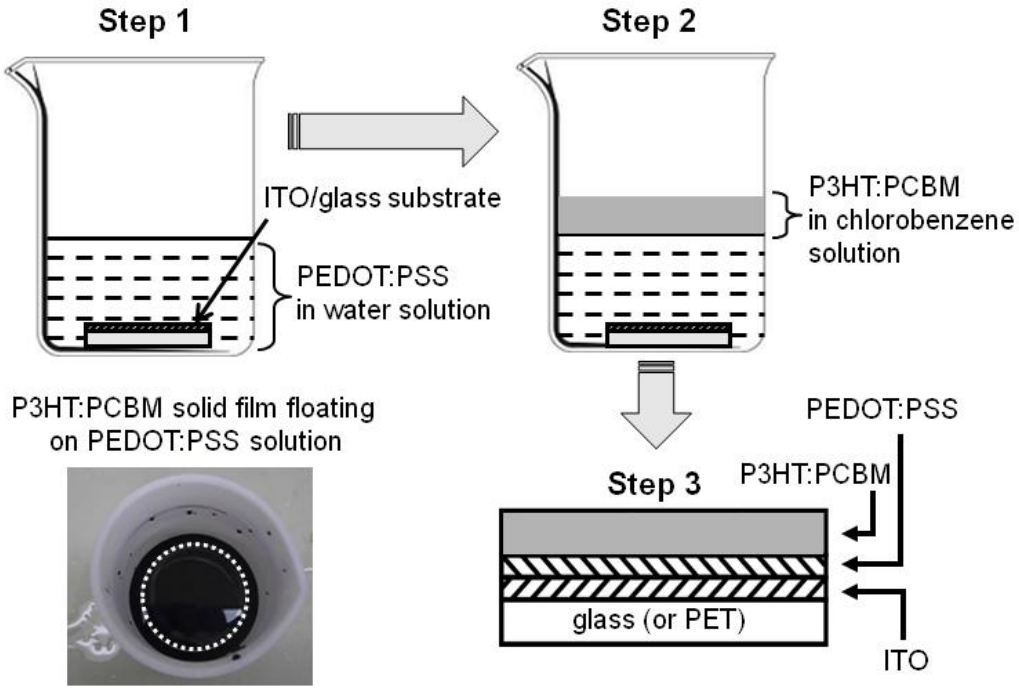

Figure 4-1. Scheme for preparing ITO/PEDOT:PSS/P3HT:PCBM multi-layered structure. PEDOT:PSS/P3HT:PCBM layered film was transferred to the ITO/glass substrate by Steps 1-3. The photograph shows a P3HT:PCBM solid film floating on a black PEDOT:PSS water solution.

4.3 Informations of chemicals and equipments

For these experiments, P3HT (99.995%, Mn = 30000-60000), PCBM (99.5%), chlorobenzene (99.8%) were purchased from Sigma-Aldrich. PEDOT:PSS solution (1.6 wt%) and oxalic acid (98%) were supplied from HC Strack and Wako Chemicals, respectively. Acetone (99.8%) and isopropanol (99.9%) were obtained from Kanto

Chemical Co., Inc. The molecular structures and energy level of each part of the fabricated device are shown in Figure 4-2.

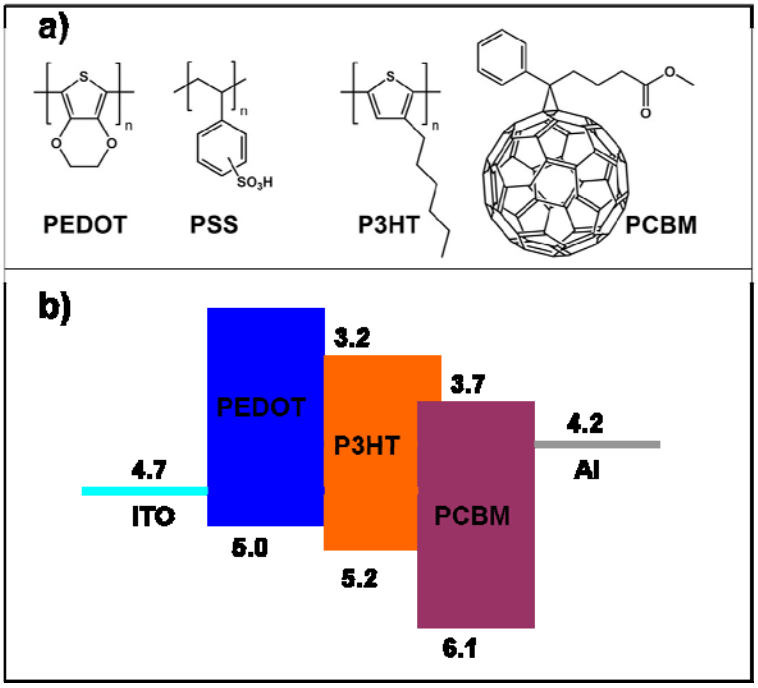

Figure 4-2. (a) Molecular structures of PEDOT, PSS, P3HT and PCBM. (b) Schematic energy level diagram of each part of the fabricated cell.

For fabrication of floating films, none special equipment was employed. Only a breaker was used as the POEDT:PSS solution container. The ITO layers on quartz substrates were deposited on the quartz substrate with a CFS-4ES/i-Miller sputtering system from Shibaura Mechatronics Corp.. Scanning Electron Microscopy (SEM) images were obtained with a Hitachi SU8000 Scanning Electron Microscopy. Optical absorption spectra were measured with a UV-Vis spectrophotometer (JASCO V-570). 120-nm thick Al electrode deposition was carried out in an electron beam deposition system (MB05-1018-0, Ulvac Co., Japan). X-ray diffraction (XRD) patterns were obtained with a Bruker AXS D8 X-ray

diffractometer with CuKα (λ =1.54056 Å) as the X-ray source. A current-voltage curve was measured with a WXS-90S-L2 super solar simulator (WACOM, Fukaya, Japan).

4.4 Experimental details

4.4.1 Fabrication of ITO/PEDOT:PSS/PCBM:P3HT structure

ITO/glass substrates were etched in 0.3M oxalic acid using a tape mask to prepare ITO patterns in small size (2 mm × 7 mm). Each patterned substrates was cleaned for 10 min with acetone, isopropanol and pure water in an ultrasonication bath.

P3HT and PCBM solutions were obtained by dissolving P3HT and PCBM, respectively, in chlorobenzene. P3HT solutions were formed with 3 and 1.5 wt. % concentrations, and the PCBM solution had a 3 wt. % concentration. All the solutions were stirred for 24 hours at 60 ^{o}C. The 3 wt. % P3HT and PCBM solutions were mixed with a ratio of 1:1 (in weight) to prepare a P3HT:PCBM solution, and then stirred for 6 hours at 60 ^{o}C. The 1.5 wt. % P3HT and P3HT:PCBM solutions were filtered with a polytetrafluoroethene syringe filter (Φ 0.2 μm, Whatman). The PEDOT:PSS solution was filtered with a polyvinylidene difluoride syringe filter (Φ 0.45 μm, Whatman).

ITO/PEDOT:PSS/PCBM:P3HT structure was obtained as described in section 4.2. After droping on PEDOT:PSS solution surface, the P3HT:PCBM droplet (5 μL) spread immediately and subsequently formed a floating solid film with a uniform thickness after the solvent had evaporated. After the substrate picked up from the PEDOT:PSS solution so that the floating P3HT:PCBM film could be transferred onto the substrate surface. For clearly understanding in the discussion section, the thus formed ITO/PEDOT:PSS/PCBM:P3HT structure is named Scheme 1.

4.4.2 Fabrication of P3HT film on water surface and fabrication of P3HT:PCBM films on water surface

For a better understanding of the process of Scheme 1, we carried out two supporting experiments. We prepared P3HT films by dropping P3HT/chlorobenzene solution (5 μl) on a water surface (Experiment S1) and prepared P3HT:PCBM films by dropping P3HT:PCBM/chlorobenzene solution (5 - 15 μl) on a water surface (Experiment S2). The components used for each experiment are summarized in Table 4-1.

Table 4-1. Components of each experiment

	Experiment S1	Experiment S2	Scheme 1
Nonaqueous phase	P3HT in chlorobenzene	P3HT:PCBM in chlorobenzene	P3HT:PCBM in chlorobenzene
Aqueous phase	Water	Water	PEDOT:PSS in water

4.4.3 Fabrication of P3HT film and P3HT:PCBM films transferred to quartz substrates

To carry out Uv-vis measurement, ITO coated quartz substrates were used to repeat Experiment S1 and Experiment S2. Quartz substrates were used to minimize the effect of absorption by the substrate because an ITO/glass substrate absorbs light in the 200 to 300 nm range. Besides, a PEDOT:PSS covered ITO/quartz sample was also prepared for comparison.

4.4.4 Fabrication of OPV device and performance measurement

A 120-nm thick Al electrode was deposited on the sample fabricated following Scheme 1. Performance measurement was performed under AM 1.5 irradiation (100 mW/cm^2) with a 0.03 cm^2 active surface area.

4.5 Results and discussion

4.5.1 Understanding of the floating phenomenon

When P3HT:PCBM solution was dropped on the PEDOT:PSS solution surface, the resulting interface was a very complicated system because there were 6 different materials: PEDOT, PSS, water, P3HT, PCBM and chlorobenzene. At room temperature, chlorobenzene is denser (1.107 g/mL) than pure water (0.98 g/mL), and they are immiscible. So chlorobenzene cannot float on the surface of water. However, we discovered that P3HT:PCBM/chlorobenzene solution (1.5 wt. %) could float on the PEDOT:PSS/water solution (1.6 wt. %) and it spread immediately to form a continuous solution layer. And then, a continuous solid film could be obtained after solvent evaporation. To form the P3HT:PCBM film on the PEDOT:PSS solution surface, the aqueous phase (PEDOT:PSS in water) must be denser than the nonaqueous phase (P3HT:PCBM in chlorobenzene), unlike the case with water and chlorobenzene. A P3HT:PCBM chlorobenzene solution can float on a PEDOT:PSS water solution, and even on pure water. We believe there are two possible reasons for this phenomenon. One is swelling, which always happens to polymers with a high molecular weight. The introduction of P3HT and PCBM led to a noticeable reduction in the density of the nonaqueous phase. The other possible reason is the surface tension at the interface between P3HT:PCBM chlorobenzene solution and PEDOT:PSS water solution.

4.5.2 P3HT film formed on water surface (Experiment S1)

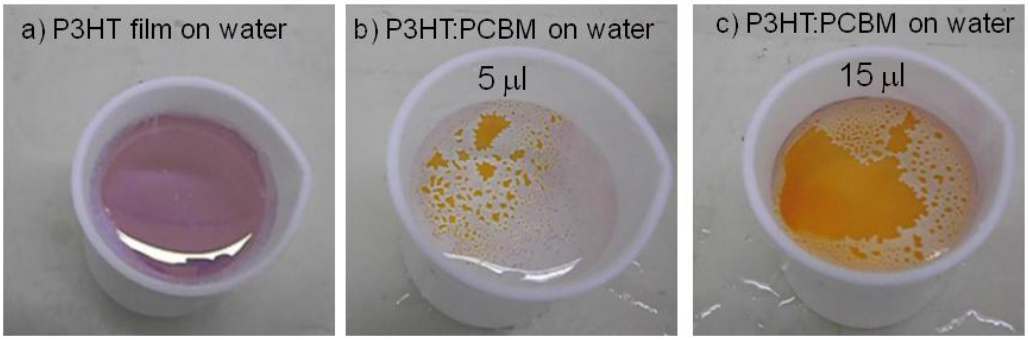

Figure 4-3. (a) Neat P3HT film fabricated on a water surface formed by dropping 5 μl of P3HT chlorobenzene solution. P3HT:PCBM islands fabricated on the water surface formed from (b) 5 μl and (c) 15 μl of P3HT:PCBM chlorobenzene solution.

P3HT lamellae have a preferential orientation, where the polymer backbone is parallel to the SiO_2 substrate or to the spin-coated PEDOT:PSS films [17,18]. The cause of this preferred alignment is not fully understood, but it has been hypothesized that it may result from an interaction between the hydrophobic P3HT side-chains and the hydrophilic substrate. In Experiment S1, a P3HT/chlorobenzene solution (1.5 wt. %, 0.945 g/ml) formed a uniform continuous film on a pure water surface (Figure 4-3a). The P3HT molecular alignment and orientation in thus prepared film are considered to be , and only to be, same as those on a SiO_2 substrate or on spin-coated PEDOT:PSS films. This preferential orientation can be inferred from the presence of an exclusive diffraction peak at $2\theta = 5.2^{\circ}$ in an XRD pattern as shown by the blue line in Figure 4-4a. The absence of the peak at 24º manifested the preferential orientation was the one and only orientation of P3HT molecules, namely, the formed film was anisotropic. Meanwhile, the absorption peak around 510 nm and a shoulder at 610 nm were observed as shown by the blue line in Figure 4-4b (see the blue arrows), indicating that the P3HT backbones are highly stacked and aligned [19]. These experimental results suggest that gradual solvent evaporation provided a mild process whereby P3HT polymer chains align parallel to the water surface driven by the π stacking. Then, the alkyl chains of P3HT come in contact at the water surface. We

consider that the surface tension thus induced at the hydrophobic alkyl chain/water interface is the driving force allowing the P3HT chlorobenzene solution to spread on water. The regular alignment of P3HT molecules is illustrated in Figure 4-5.

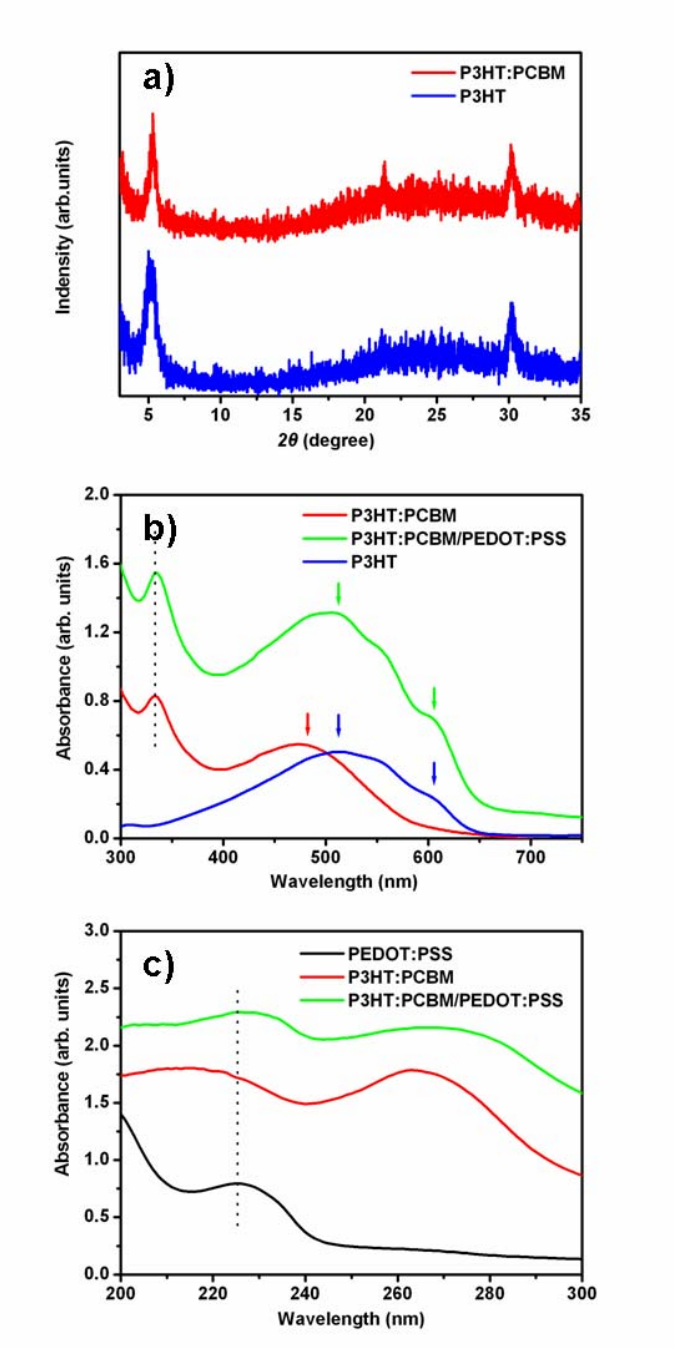

Figure 4-4. (a) X-ray diffraction patterns of neat P3HT film and P3HT:PCBM composite film prepared by floating P3HT solution and P3HT:PCBM solution, respectively, on a water surface,. (b) UV-Vis absorption spectra in the 300 to 750 nm range of the neat P3HT film (blue), P3HT:PCBM composite film (red) and PEDOT:PSS/ P3HT:PCBM composite film (green). (c) Absorption spectra in the 200 to 300 nm range of the PEDOT:PSS (black), P3HT:PCBM composite film (red) and PEDOT:PSS/ P3HT:PCBM composite film (green).

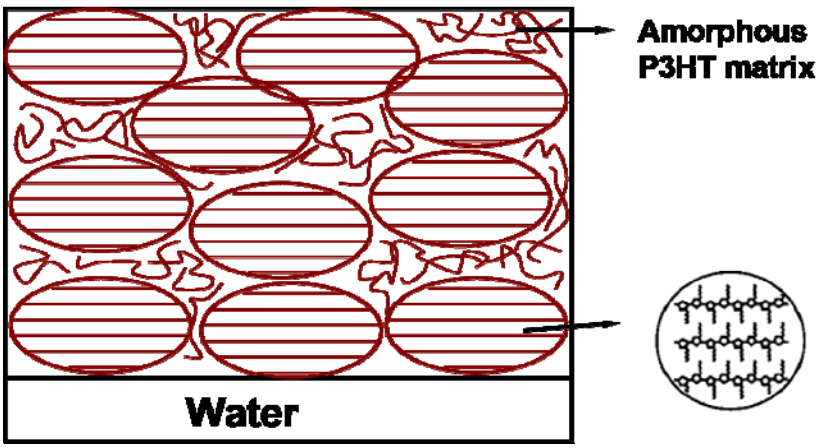

Figure 4-5. Illustration of P3HT film on water surface. P3HT molecules have highly regular alignment.

4.5.3 Effect of PCBM on morphologies of P3HT:PCBM films on water surface (Experiment S2)

The blending of PCBM molecules into P3HT complicates the situation because the two compounds separate from each other and PCBM aggregates disturb the P3HT molecular alignment [20]. In fact, dozens of discontinuous islands were formed as can be seen in Figure 4-3b when a small droplet of P3HT:PCBM solution (5 μl, 0.955 g/mL) was dropped on the water surface. Even though a large-scale continuous film was formed at the center of the surface (Figure 4-3c) as the volume of the P3HT:PCBM droplets increased to 15 μl, the

film morphology was totally different from that of the neat P3HT film formed on the water surface (Figure 4-3a).

The P3HT:PCBM film thus prepared exhibited a blue shift of 20 to 490 nm in the absorption peak (see the red arrow in Figure 4-4b) compared with the spectrum obtained in Experiment S1. And the shoulder at 610 nm disappeared, proving that the introduction of PCBM degraded the P3HT backbone alignment by penetrating. The two activities, aggregation and penetration, caused that the net-work nano-structure is formed. On the other hand, a diffraction peak was observed at $2\theta = 5.2^{\circ}$ in the XRD pattern (red line in Figure 4-4a), meaning that the P3HT backbone was still mainly parallel to the water surface. That is, the surface tension at the alkyl chain/water interface still enables the P3HT:PCBM film to float on water. On the other hand, PCBM aggregates prevent the formation of continuous networks of P3HT polymer chains. This is illustrated in Figure 4-6.

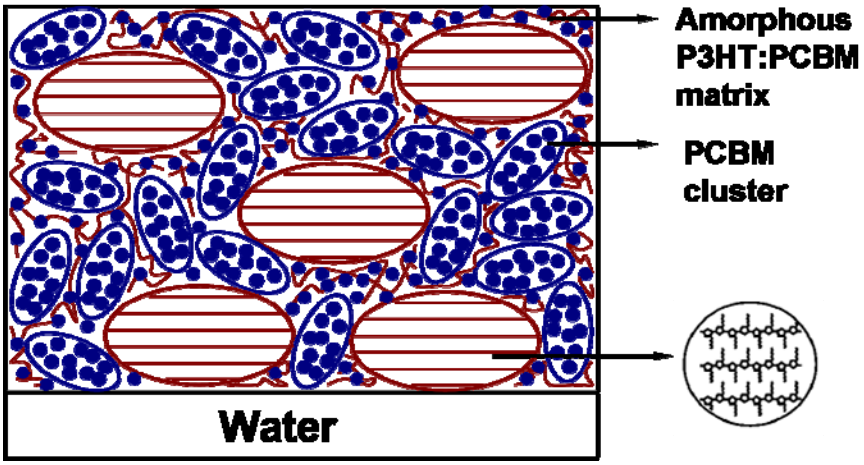

Figure 4-6. Illustration of P3HT:PCBM film formed on water surface. The introduction of PCBM disturbed P3HT forming continuous networks because of it aggregateion.

4.5.4 Effect of PEDOT:PSS on formation of continuous P3HT:PCBM/PEDOT:PSS composite film (Scheme 1)

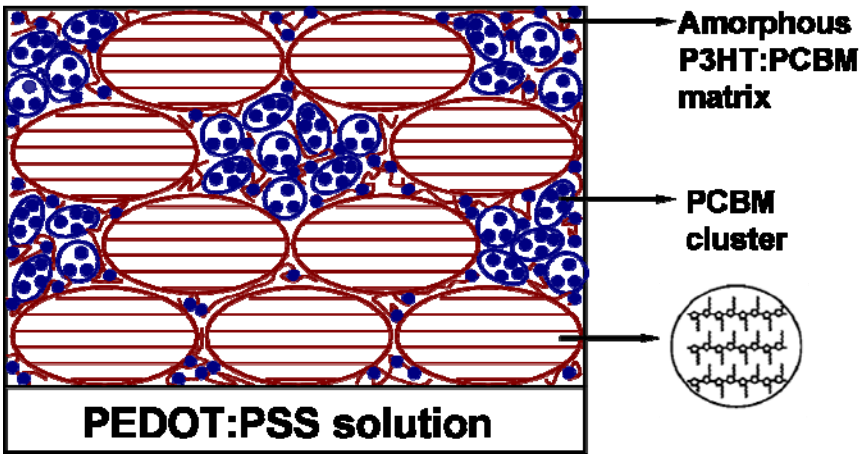

Figure 4-7. Illustration of P3HT:PCBM film formed on the surface of PEDOT:PSS solution. The introduction of PEDOT:PSS solution decreased the influence of PCBM.

As shown in the photograph in Figure 4-1, the P3HT:PCBM chlorobenzene solution spread instantly when dropped on the PEDOT:PSS water solution (1.05 g/ml) surface. Then, a continuous film was formed that covered the entire container area (Scheme 1) in a similar manner to neat P3HT film on water (Figure 4-3a). The absorption spectra of this P3HT:PCBM/PEDOT:PSS composite film are shown by the green lines in Figure 4-4b (300-750 nm) and c (200-300 nm). The absorption peak at about 510 nm showed a red shift of 20 nm compared with that obtained in Experiment S2 and a shoulder appeared at 610 nm (see the green arrows in Figure 4-4b). These results confirmed that the P3HT chain alignment was improved [19]. These variations are assumed to result from the fact that that the PEDOT:PSS reduced the amount of disturbance that PCBM caused the P3HT alignment, in other words, it enhanced the regular alignment of the P3HT polymer chains. The mechanism is not clear but one possibility is that some of the PCBM molecules diffused into the PEDOT:PSS layer as the result of an instantaneously induced dipole

interaction when the P3HT:PCBM droplet touched the PEDOT:PSS solution. This is similar to the PCBM molecules penetrating the PEDOT:PSS during the annealing process [21]. As a result, the P3HT polymer networks extended and the P3HT/water contact area increased. Consequently, a continuous P3HT:PCBM film with an improved orientation was obtained as in Experiment S1. Figure 4-7 illustrates the formed continuous P3HT:PCBM film formed on the surface of PEDOT:PSS solution.

Absorption spectra were obtained to confirm the presence of the PEDOT:PSS layer in the multi-layered film fabricated in Scheme 1. Characteristic PCBM absorption peaks were observed around 268 and 335 nm as indicated by the dotted lines in Figure 4-4c and b [22, 23]. The peaks showed no shift after the composition of P3HT:PCBM film with a PEDOT:PSS layer. The peak at 225 nm seen in Figure 4-4c is attributed to the π and π* transitions of benzene rings, which is characteristic of the PSS system [24]. This peak directly demonstrates the presence of PEDOT:PSS. Here, P3HT:PCBM is insoluble in water and PEDOT:PSS is insoluble in chlorobenzene. Therefore, it is reasonable to conclude that the P3HT:PCBM and PEDOT:PSS films were layered in a sequential order.

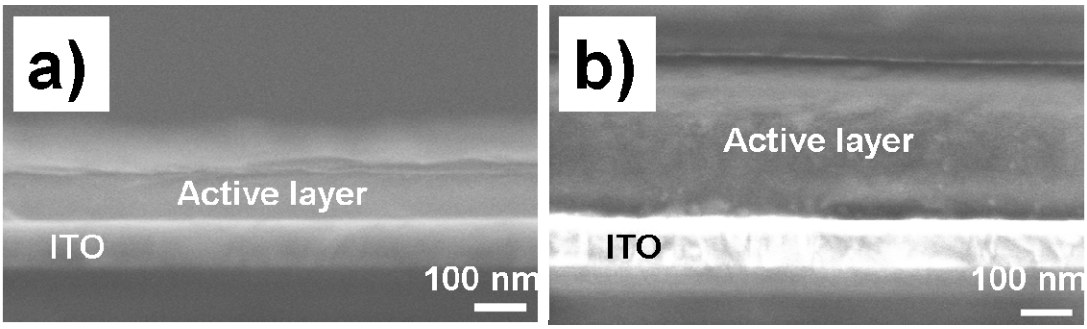

Figure 4-8. Cross-section of SEM images of P3HT:PCBM films fabricated by a) 5 µl of solution and b) 15 µl of solution. The thickness is ca. 80 nm and 260 nm, respectively.

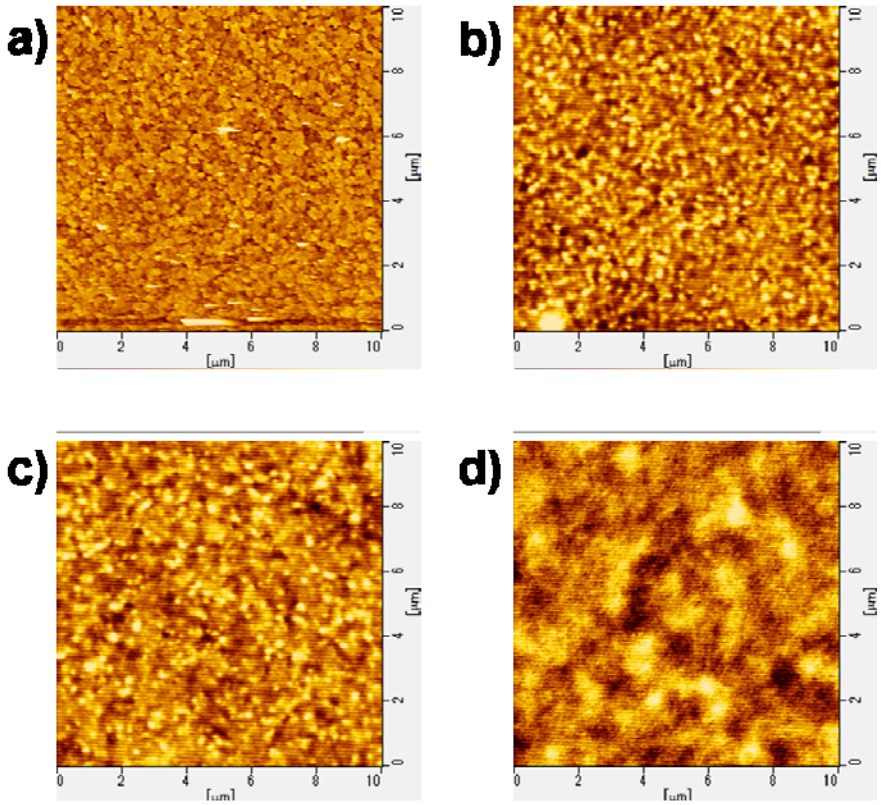

Figure 4-9. AFM images of a) ITO substrate and P3HT:PCBM films fabricated with solution of b) 5 µl, c)10µl and d) 15 µl. (10 µm × 10 µm for each image)

It appears that the final area of the P3HT:PCBM film is determined by the container cross sectional area. And the film thickness depends on the volume of the P3HT:PCBM solution droplet. In our study, we used a 5 cm diameter beaker and 5 - 15 µl of P3HT:PCBM solution droplets were droped. Then, we confirmed that the film thickness was controllable in the 80 to 260 nm range according to the droplet volume (Figure 4-8) and the surface smooth could be controlled no worse than ITO substrate (Figure 4-9, Table 4-2).

Table 4-2. Root-mean-square (RMS) of ITO substrate and films formed with different solution volume

Sample	ITO	Volume: 5 µl	Volume 10 µl	Volume: 15 µl
RMS	2.748	3.151	2.113	1.700

4.5.5 Device performance

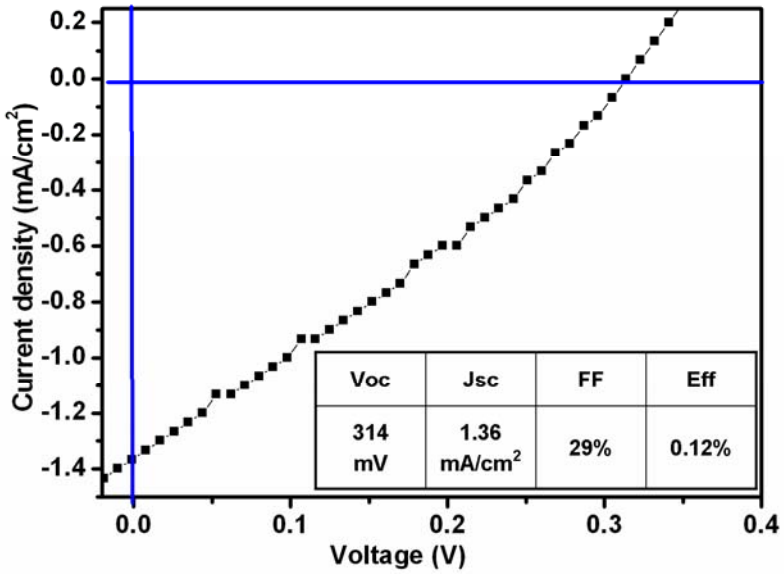

Figure 4-10. *I-V* curve of the ITO/PEDOT:PSS/P3HT:PCBM/Al photovoltaic device. The device properties are summarized in the table.

Finally, we examined the photovoltaic effect of the P3HT:PCBM/PEDOT:PSS film. Prior to the measurement, a sample on a commercially available glass/ITO substrate was placed in a wide-mouth bottle along with a small bottle containing 50 µl chlorobenzene for

1 hour to improve the ordering of the polymer chains [25]. Figure 4-10 shows a current-voltage (I-V) curve. This measurement was performed under AM 1.5 irradiation (100 mW/cm^2) with a 0.03 cm^2 active surface area. The device properties are summarized in the table in Figure 4-10. The poor performance might be attributed to the preparation process during which there was some residual water sealed in the underlying PEDOT:PSS layer by the P3HT:PCBM film. The moisture may lead to a poor interface contact. Nevertheless, this result demonstrates that the thus fabricated ITO/PEDOT:PSS/P3HT:PCBM structure can yield a photovoltaic effect.

4.6 Summary

We developed a simple one-step technique for fabricating a large-scale ITO/PEDOT:PSS/P3HT:PCBM structure by transferring a floating P3HT:PCBM film onto an ITO coated glass substrate from a PEDOT:PSS solution. We discussed potential factors that would enable the film to float on the solution, namely swelling resulting in decreased density and surface tension at the alkyl chain/water interface. The formed ITO/PEDOT:PSS/P3HT:PCBM structure was used to fabricate photovoltaic device. The device properties determined in this study are preliminary and there is still room for further improvement.

4.7 Motivations and significances of this work

Developing easy fabrication technique to lower cost is another aspect for development of organic solar cells. The floating technique demonstrated in this chapter can be summarized in " fabrication in large scale by cheap method". The structure can be obtained without the need for costly equipment and can be fabricated with a large area depending on the container area. Another advantage of this technique is that the film can be formed with

almost no waste of materials. Moreover, the active layer thickness can be controlled by adjusting the volume of the P3HT:PCBM solution. Films prepared in the above way were confirmed to have a very uniform thickness. Additionally, this technique is easy to use on substrates made of soft materials such as PET. For further development, a replaceable solvent which can take the place of water and minimize the negative effect of moisture is essential.

References

[1] Krebs, F. C. Fabrication and Processing of Polymer Solar Cells: A Review of Printing and Coating Techniques. *Sol. Energ. Mat. Sol. C* **2009**, *93*, 394-412.

[2] Helgesen, M.; Søndergaard, R.; Krebs, F. C. Advanced Materials and Processes for Polymer Solar Cell Devices. *J. Mater. Chem.* **2010**, *20*, 36-60.

[3] Krebs, F. C.; Gevorgyan, S. A.; Alstrup, J. A Roll-to-roll Process to Flexible Polymer Solar Cells: Model Studies, Manufacture and Operational Stability Studies. *J. Mater. Chem.* **2009**, *19*, 5442.

[4] Liang, Y.; Xu, Z.; Xia, J.; Tsai, S. T.; Wu, Y.; Li, G.; Ray, C.; Yu, L. For the Bright Future-Bulk Heterojunction Polymer Solar Cells with Power Conversion Efficiency of 7.4%. *Adv. Mater.* **2010**, *22*, E135-138.

[5] Chen, H. Y.; Hou, J.; Zhang, S.; Liang, Y.; Yang, G.; Yang, Y.; Yu, L.; Wu, Y.; Li, G. Polymer Solar Cells with Enhanced Open-circuit Voltage and Efficiency. *Nat. Photonics* **2009**, *3***,** 649-653.

[6] Norrman, K.; Ghanbari-Siahkali, A.; Larsen, N. B. Studies of Spin-coated Polymer Films. *Annu. Rep. Prog. Chem. Sect. C* **2005**, *101*, 174-201.

[7] Hoth, C. N.; Choulis, S. A.; Schilinsky, P.; Brabec, C. J.; High Photovoltaic Performance of Inkjet Printed Polymer:Fullerene Blends. *Adv. Mater.* **2007**, *19*, 3973-3978.

[8] Aernouts, T.; Aleksandrov, T.; Girotto, C.; Genoe, J.; Poortmans, J. Polymer Based Organic Solar Cells Using Ink-jet Printed Active Layers. *Appl. Phys. Lett.* **2008**, *92*, 033306.

[9] Steirer, K. X.; Reese, M. O.; Rupert, B.; Kopidakis, N.; Olson, D. C.; Collins, R. T.; Ginley, D. S. Ultrasonic Spray Deposition for Production of Organic Solar Cells. *Sol. Energ. Mat. Sol. C.* **2009**, *93*, 447-453.

[10] Girotto, C.; Rand, B. P.; Genoe, J.; Heremans, P. Exploring Spray Coating as a Deposition Technique for the Fabrication of Solution-processed Solar Cells. *Sol. Energ. Mat. Sol. C.* **2009**, *93*, 454-458.

[11] Vak, D.; Kim, S.; Jo, J.; Oh, S.; Na, S.; Kim, J.; Kim, D. Fabrication of Organic Bulk Heterojunction Solar Cells by a Spray Deposition Method for Low-cost Power Generation.

Appl. Phys. Lett. **2007**, *91*, 081102.

[12] Krebs, F. C.; Jørgensen, M.; Norrman, K.; Hagemann, O.; Alstrup, J.; Nielsen, T. D.; Fyenbo, J.; Larsen, K.; Kristensen, J. A Complete Process for Production of Flexible Large Area Polymer Solar Cells Entirely Using Screen Printing-First Public Demonstration. *Sol. Energ. Mat. Sol. C.* **2009**, *93*, 422-441.

[13] Shaheen, S. E.; Radspinner, R.; Peyghambarian, N.; Jabbour, G. E. Fabrication of Bulk Heterojunction Plastic Solar Cells by Screen Printing. *Appl.Phys. Lett.* **2001**, *79*, 2996.

[14] Krebs, F. C.; Alstrup, J.; Spanggaard, H.; Larsen, K.; Kold, E. Production of Large-area Polymer Solar Cells by Industrial Silk Screen Printing, Lifetime Considerations and Lamination with Polyethyleneterephthalate. *Sol. Energ. Mat. Sol. C.* **2004**, *83*, 293-300.

[15] Hu, Z.; Zhang, J.; Xiong, S.; Zhao, Y. Performance of Polymer Solar Cells Fabricated by Dip Coating Process. *Sol. Energ. Mat. Sol. C.* **2012**, *99*, 221-225.

[16] Valentini, L.; Bagnis, D.; Kenny, M. Nanofibrillar Self-organization of Regioregular Poly(3-hexylthiophene) and [6,6]-phenyl C_{61}-butyric Acid Methyl Ester by Dip-coating: A Simple Method to Obtain Efficient Bulk Heterojunction Solar Cells. *Nanotechnology* **2009**, *20*, 095603.

[17] U. Zhokhavets, T. Erb, H. Hoppe, G. Gobsch, N. S. Sariciftci, Effect of Annealing of Poly(3-hexylthiophene)/Fullerene Bulk Heterojunction Composites on Structural and Optical Properties. *Thin Solid Films* **2006**, *496*, 679-682.

[18] Erb, T.; Zhokhavets, U.; Gobsch, G.; Raleva, S.; Stuhn, B.; Schilinsky, P.; Waldauf, C.; Brabec, C.; Correlation Between Structural and Optical Properties of Composite Polymer/Fullerene Films for Organic Solar Cells. Adv. Funct. Mater. **2005**, *15*, 1193-1196.

[19] Baek, W. H.; Yang, H.; Yoon, T. S.; Kang, C. J.; Lee, H. H.; Kim, Y. S. Effect of P3HT:PCBM Concentration in Solvent on Performances of Organic Solar Cells. *Sol. Energ. Mat. Sol. C.* **2009**, *93*, 1263-1267.

[20] Schmidt-Hansberg, B.; Sanyal, M.; Klein, M. F.; Pfaff, M.; Schnabe, N.; Jaiser, S.; Vorobiev, A.; Müller, E.; Colsmann, A.; Scharfer, P.; Gerthsen, D.; Lemmer, U.; Barrena, E.; Schabel, W. Moving through the Phase Diagram: Morphology Formation in Solution Cast Polymer–Fullerene Blend Films for Organic Solar Cells. *Acs Nano* **2011**, *5*, 8579-8590.

[21] Chirvase, D.; Parisi, J.; Hummelen, J. C.; Dyakonov, V. Influence of Nanomorphology on the Photovoltaic Action of Polymer–fullerene Composites. *Nanotechnology* **2004**, *15*, 1317.

[22] Yang, Y.; Jiang, Y.; Xu, J.; Yu, J. Preparation and Characterization of Conducting Poly(3,4-ethylenedioxythiophene)-Poly(styrenesulfonate) Langmuir–Blodgett Film. *Thin Solid Films* **2008**, *516*, 1191-1196.

[23] Swinnen, A.; Haeldermans, I.; vande Ven, M.; D'Haen, J.; Vanhoyland, G.; Aresu, S.; D'Olieslaeger, M.; Manca, J.; Tuning the Dimensions of C_{60}-Based Needlelike Crystals in Blended Thin Films. *Adv. Funct. Mater.* **2006**, *16*, 760-765.

[24] Chen, D.; Nakahara, A.; Wei, D.; Nordlund, D.; Russell, T. P. P3HT/PCBM Bulk Heterojunction Organic Photovoltaics: Correlating Efficiency and Morphology. *Nano Lett.* **2011**, *11*, 561-567.

[25] Li, G.; Yao, Y.; Yang, H.; Shrotriya, V.; Yang, G.; Yang, Y. "Solvent Annealing" Effect in Polymer Solar Cells Based on Poly(3-hexylthiophene) and Methanofullerenes. *Adv. Funct. Mater.* **2007**, *17*, 1636-1644.

Chapter 5. Conclusions and perspective

In this thesis, we employed P3HT as the main material to study its applications in organic devices base on its electrical and photoelectric properties and its processability. We focused on the dimensional control, from sub-1D to 1D and then 2D, of P3HT and explored the relevant applications.

(1) We described an AAO template technique for fabricating regular arrays of sub-1D P3HT pillars and interdigitated p-n junctions of P3HT/C_{60}. The feature of this technique is the high controllability of the nanoscale dimensions, such as the diameter, interval, height, and uniformity of the P3HT pillars. That is, these dimensions can be tailored to improve effective light absorption and carrier dissociation and transport. The device properties in this study were preliminary, and there is still room for further improvement. However, the technique we demonstrated here has great potential for use in developing a practical device because nanoscale structures can be fabricated in a large area exceeding 100 mm^2.

(2) We have demonstrated 1D P3HT/F4-TCNQ composite nanowires synthesized by employing an AAO template which have superior conductivity comparing to thin films. Four-probe STM measurements on individual molecular nanowires indicated that the synthesis approach has two distinct advantages with respect to increasing the electrical conductivity of P3HT/F4-TCNQ composite nanowires. One is that it improves the alignment of the polymer chains, and the other is that it enhances the chemical dopant. We believe that the capillary force in the nanoscale pores prevents the segregation of F4-TCNQ and enables high doping concentrations. A low resistivity of 0.16 Ω cm was achieved for the 10 wt % P3HT/F4-TCNQ composite nanowires, which was not possible with the thin film geometry.

(3) We developed a simple one-step technique for fabricating a 2D large-scale ITO/PEDOT:PSS/P3HT:PCBM structure by transferring a floating P3HT:PCBM film onto an ITO coated glass substrate from a PEDOT:PSS solution. We discussed potential factors that would enable the film to float on the solution, namely swelling resulting in decreased

density and surface tension at the alkyl chain/water interface. The structure can be obtained without the need for costly equipment and can be fabricated with a large area depending on the container area. Another advantage of this technique is that the film can be formed with almost no waste of materials. Moreover, the active layer thickness can be controlled by adjusting the volume of the P3HT:PCBM solution. Films prepared in the above way were confirmed to have a very uniform thickness. Additionally, this technique is easy to use on substrates made of soft materials such as PET. The device properties determined in this study are preliminary and there is still room for further improvement. However, the above advantages mean that the technique we demonstrated here has great potential for use in developing a practical device.

P3HT is certainly a case system to test the applicability of experimental methods and insights gained when investigating conventional polymer crystallization, for example, using epitaxial crystallization methods, self-seeding or nucleating agents. These directly impact its applications. However conjugated polymers have intrinsic characteristic that make them significantly different from more flexible polymers, especially in terms of anisotropy of interactions in the unit cell and rigidity of the conjugated backbone that impacts directly the folding ability of the chains and correspondingly the crystallization mode (folded *vs.* extended chain crystallization). From the charge transport viewpoint, one important issue remains the possibility to crystallize high-Mw P3ATs in the form of extended-chain crystalline domains, trying to reduce the level of amorphous material and promoting long range crystalline perfection. Some preliminary studies in that direction have been reported recently suggesting that high-pressure crystallization of P3HT may lead to higher charge carrier mobilities. Further improvements can be foreseen with mastering of chemical defects in the chains of P3ATs. Alonging with the development of understanding the nature of P3HT represented P3ATs, their practical applications would be extended in wider fields.

Acknowledgment

After three and a half long years, it is time to complete my Ph.D. studies. At the beginning of this program, my lack of research experience meant I had to spend much time learning about the research system. To me, pursuing a Ph.D. meant taking complete responsibility for understanding information accurately, successfully applying knowledge, designing and managing experiments in a productive manner, using research creatively in my topic selection, setting criteria to scientifically analyze results, contributing to professional society, and ensuring effective communication. I would like to thank Prof. Wakayama Yutaka and Dr. Shirai Yasuhiro for their patience and guidance during my graduate studies. Prof. Wakayama consistently showed his trust and belief in me, and this strongly motivated me to achieve my goals. I am also thankful for my committee members; Professors Adachi Chihaya and Ishihara Tatsumi deserve special thanks for their work on this thesis committee. They provided professional discussions and collaboration opportunities that I greatly appreciate. Professor Li An-ping, from Oak Ridge National Laboratory, USA, offered the help on the STM system. I am very appreciate for his help.

In addition, the support of my family was a great asset, and without it, I could not have earned this Ph.D. When I began studying in the Japan, my daughter Hu Bei was not yet born. How time has flown. She is now 8-month-old and has begun to speak. I promised to be a good father but until now I feel I did almost nothing for her, so I must thank her mother, my wife, Xu Jingjing. She is a great woman for our family. She's devotion to the raising of our child has enabled me to focus on my research more than would be possible otherwise. I give my sincerest thanks to my wife and my daughter for their big smiles and for constantly showing their love for me.

My family in China has also provided great mental support. I have encountered many hurdles during this journey, and my family's love and encouragement has kept me focused. These supports have been a great part of the world I have experienced so I am happy.

Also, my friends in Japan, Zhang Qin, Cai Rong, Oh Seungjun, Ishiguro Yasushi, Chen Peng and Kobashi Kazuyoshi, they treat me like brotherhood. We always have parties and drink together. They gave me a lot of happy time and taught me a lot including Japanese language, but I am very sorry my Japanese is still not good.

Hu Jianchen

June 12th, 2013